Received: 2 February 2021 | Revised: 22 June 2021 | Accepted: 23 June 2021

DOI: 10.1111/jnc.15461

Journal of Neurochemistry JNC The Official Journal of the International Society for Neurochemistry WILEY

ORIGINAL ARTICLE

Brain iron enrichment attenuates α-synuclein spreading after injection of preformed fibrils

Karina Dauer née Joppe[1,2] | Lars Tatenhorst[1,2] | Lucas Caldi Gomes[1,2,3] | Shuyu Zhang[3] | Mojan Parvaz[3] | Eleonora Carboni[1] | Anna-Elisa Roser[1,2] | Hazem El DeBakey[4] | Mathias Bähr[1,2,5] | Katarina Vogel-Mikuš[6,7] | Chi Wang Ip[4] | Stefan Becker[8] | Markus Zweckstetter[1,9,10] | Paul Lingor[1,2,3]

[1]Department of Neurology, University Medical Center Goettingen, Goettingen, Germany

[2]Center for Biostructural Imaging of Neurodegeneration, University Medical Center Goettingen, Goettingen, Germany

[3]Department of Neurology, School of Medicine, University Hospital rechts der Isar, Technical University of Munich, Munich, Germany

[4]Department of Neurology, University Hospital of Wuerzburg, Wuerzburg, Germany

[5]Cluster of Excellence "Multiscale Bioimaging: from Molecular Machines to Networks of Excitable Cells" (MBExC), University of Goettingen, Goettingen, Germany

[6]Biotechnical faculty, University of Ljubljana, Ljubljana, Slovenia

[7]Jozef Stefan Institute, Ljubljana, Slovenia

[8]Department of NMR Based Structural Biology, Max Planck Institute for Biophysical Chemistry, Goettingen, Germany

[9]German Center for Neurodegenerative Diseases (DZNE), Goettingen, Germany

[10]Research group Mass Spectrometry, Max Planck Institute for Biophysical Chemistry, Goettingen, Germany

Correspondence
Paul Lingor and Lars Tatenhorst, Department of Neurology, School of Medicine, University Hospital rechts der Isar, Technical University of Munich, Ismaninger Straße 22, 81675 Munich, Germany.
Email: paul.lingor@tum.de lars.tatenhorst@med.uni-goettingen.de

Funding information
Deutsche Forschungsgemeinschaft, Grant/Award Number: CNMPB and EXC 2067/1- 390729940; MPI

Read the Editorial article on page 414.

Abstract

Regional iron accumulation and α-synuclein (α-syn) spreading pathology within the central nervous system are common pathological findings in Parkinson's disease (PD). Whereas iron is known to bind to α-syn, facilitating its aggregation and regulating α-syn expression, it remains unclear if and how iron also modulates α-syn spreading. To elucidate the influence of iron on the propagation of α-syn pathology, we investigated α-syn spreading after stereotactic injection of α-syn preformed fibrils (PFFs) into the striatum of mouse brains after neonatal brain iron enrichment. C57Bl/6J mouse pups received oral gavage with 60, 120, or 240 mg/kg carbonyl iron or vehicle between postnatal days 10 and 17. At 12 weeks of age, intrastriatal injections of 5-μg PFFs were performed to induce seeding of α-syn aggregates. At 90 days post-injection, PFFs-injected mice displayed long-term memory deficits, without affection of motor behavior. Interestingly, quantification of α-syn phosphorylated at S129 showed reduced

Abbreviations: ANOVA, analysis of variance; AraC, cytosine arabinoside-containing medium; BSA, bovine serum albumin; bw, body weight; cat. no., catalogue number; DAB, diaminobenzidine-HCl; DAPI, 4′,6-diamidino-2-phenylindole; div, day in vitro; dpi, days post-injection; E 18.5, embryonic day 18.5; FCS, fetal calf serum; IVC, individually ventilated cages; LTM, long-term memory; NGS, normal goat serum; NOR, novel object recognition; ns, not significant; PBS, phosphate-buffered saline; PD, Parkinson's disease; PFA, paraformaldehyde; PFFs, preformed fibrils; ROI, region of interest; rpm, rotations per minute; RRID, see scicrunch.org, Research Resource Identifier; SDD, silicon drift detector; *SEM*, standard error of the mean; SN, substantia nigra; STM, short-term memory; XRF, X-ray fluorescence; α-syn, α-synuclein.

Karina Dauer née Joppe and Lars Tatenhorst contributed equally to this study.

α-syn pathology and attenuated spreading to connectome-specific brain regions after brain iron enrichment. Furthermore, PFFs injection caused intrastriatal microglia accumulation, which was alleviated by iron in a dose-dependent way. In primary cortical neurons in a microfluidic chamber model in vitro, iron application did not alter transsynaptic α-syn propagation, possibly indicating an involvement of non-neuronal cells in this process. Our study suggests that α-syn PFFs may induce cognitive deficits in mice independent of iron. However, a redistribution of α-syn aggregate pathology and reduction of striatal microglia accumulation in the mouse brain may be mediated via iron-induced alterations of the brain connectome.

KEYWORDS
alpha-synuclein, alpha-synuclein propagation, alpha-synuclein seeding, iron dyshomeostasis, Parkinson's disease

1 | INTRODUCTION

Parkinson's disease (PD) is a progressive neurodegenerative disorder with high socioeconomic relevance and an increasing number of patients affected worldwide. So far, PD can neither be prevented nor cured, and biomarkers for accurate and early-onset identification of the disease are still missing. Its pathophysiology is only incompletely understood, but there is evidence to suggest that axonal degeneration precedes neuronal cell loss in PD (Burke and O´Malley 2014) and that initial pre-motor symptoms precede the onset of motor deficits by many years (Berg et al., 2012). Lewy bodies, intracytoplasmic protein inclusions containing α-synuclein (α-syn) as one of the main components, are found in different brain regions of PD patients and α-syn pathology can be used for pathological disease staging (Braak et al., 2003). In PD brains, the natively unfolded α-syn protein is found in pathological conformations as misfolded beta-sheets and fibrils (Spillantini et al., 1998). Oligomers and fibrils of α-syn are thought to be neurotoxic and are presumed to spread throughout the brain of PD patients along neuroanatomical connections (Henderson et al., 2019; Peelaerts et al., 2015; Winner & Jappelli, 2011).

Stereotactic injections of α-syn preformed fibrils (PFFs) into various brain regions of mice or rats have been used to investigate the propagation and transmission of α-syn PFFs through the brain (Zhang et al., 2019). Several studies revealed progressive spreading of PFFs, alterations in the behavior of the animals as well as progressive neurodegeneration, depending on the amount of PFFs injected, animal genotype, injected region, and time after injection (Luk, Kehm, Carroll, et al., 2012; Masuda-Suzukake et al., 2013; Paumier et al., 2015).

The accumulation of iron in the substantia nigra (SN) is another neurochemical hallmark in the brains of PD patients (Dexter et al., 1991; Rossi et al., 2013). Using magnetic resonance imaging, iron accumulation has been observed in the brains of PD patients (Rossi et al., 2013). α-syn has binding sites for iron and studies show that iron may foster α-syn aggregation (Golts et al., 2002; Uversky et al., 2001). In addition to the formation of aggregates triggered by the direct binding of iron to α-syn, elevated levels of iron are also known to lead to increased oxidative stress (produced in the iron-catalyzed Fenton and Haber–Weiss reactions), a process that may indirectly contribute to the misfolding of α-syn (Joppe et al., 2019). Interestingly, iron chelators were already shown to decrease the iron content in animal models of PD and improve behavioral outcomes (Carboni et al., 2017), and the disease-modifying effects of the iron-chelator Deferiprone were already investigated in clinical trials in PD patients (Devos et al., 2014; ClinicalTrials.gov. National Library of Medicine (U.S.) 2015; Martin-Bastida et al., 2017).

Aiming to better understand the contribution of iron to the propagation of α-syn pathology, we investigated the spreading of α-syn after stereotactic injection of PFFs into the striatum of mice with neonatal brain iron enrichment.

2 | MATERIALS AND METHODS

2.1 | Preparation of α-syn PFFs

Both human and mouse α-syn were expressed recombinantly in *Escherichia coli* strain BL21(DE3) (cat. no. C2527H, New England Biolabs) and purified as described previously (Hoyer et al., 2002). Briefly, the cells from 1 L minimal medium expression culture wereThe usage “the cells from 1 L minimal medium expression culture” is not clear. Please check. lysed by freeze–thaw cycles followed by sonication, boiled for 15 min and centrifuged at 48.000 *g* for 45 min. From the supernatant DNA was precipitated by adding streptomycin (10 mg/ml) to the ice-cold stirred solution. After another centrifugation step, α-syn was precipitated from the supernatant by adding ammonium sulfate to 0.36 g/ml. The pellet was resuspended in 25 mM Tris/HCl, pH 7.7 and further purified by anion-exchange chromatography on a 30-mm POROS HQ column (cat. no. 1232212, PerSeptive Biosystems). To prepare monomeric α-syn without any aggregates, the protein was dialyzed against phosphate-buffered saline (PBS;

cat. no. A0964, Applichem) buffer, pH 7.4, centrifuged at 106,000 *g* for 1 hr at 4°C and filtrated through 0.22-μm ULTRAFREE-MC centrifugal filter units (cat. no. UFC30GV0S, Merck Millipore). The final protein concentration was set to 5 mg/ml.

For fibrillization in PBS buffer, monomeric human and mouse α-syn were incubated at 37°C with constant stirring at 200 rotations per minute (rpm). Progress of fibrillization was monitored with a thioflavin T fluorescence assay as described before (Hoyer et al., 2004). Briefly, a 1–2 μl aliquot of fibrils was mixed with 2 ml of a solution of 5 μM thioflavin T (cat. no. T3516, Sigma) in 50 mM glycine/NaOH, pH 8.2, at different incubation times and the fluorescence emission was measured between 460 and 600 nm on a Varian Cary Eclipse fluorescence spectrophotometer (Agilent Technologies). Fibrillization of human α-syn reached steady state after 7–9 days while fibrillization of mouse α-syn took up to 11 days. Monomeric protein and PFFs were shock frozen in liquid nitrogen and stored at −80°C until usage. Immediately before usage, PFFs were diluted to the final concentration and sonicated (30 s, 1 cycle, 10% power; Bandelin SonoPlus). Electron microscopy images were acquired from PFFs before and after sonication (Figure S1). PFFs were applied to 400-mesh copper grids (cat. no. G2400C, Plano) and stained with 1% uranyl acetate (cat. no. 8473, Merck). Images were acquired using a Philips CM120 electron microscope (Philips) equipped with a TemCam 224A slow scan CCD camera (TVIPS) at a defocus of 2.3 μm, as previously described (Tatenhorst et al., 2016). For all cell culture experiments, mouse-derived α-syn PFFs were employed. For all animal experiments, human-derived monomeric α-syn and α-syn PFFs were employed.

2.2 | Animal experiments

Wild-type C57Bl/6J mouse (RRID: IMSR_JAX:000664) couples purchased from Charles River were used for breeding in the Central Animal Care Unit of the University Medical Center Goettingen, Germany. The study received approval from the institutional ethics committee and the animals were treated according to the regulations of the local animal research council and legislation of the State of Lower Saxony, Germany (ethics approval number: 33.9-42502-04-15/1982) in an exploratory study. Sample size calculations were performed using GPower 3.1 software (Faul et al., 2009) according to the guidelines of the legislation of the State of Lower Saxony, Germany (ANOVA, a-priori analysis, effect size f = 0.4, power = 0.8). Mice were housed in individually ventilated cages (IVC, Tecniplast) with standard ad libitum food, water, and 12-hr dark/light cycle. No randomization was performed to allocate subjects in the study, no exclusion criteria were pre-determined. Altogether 233 animals (127 males, 106 females) were used in this study. The average body weight of all mice was 26.2 g, the number of animals used per group is indicated in the figure legends. This study was not pre-registered.

Female and male mouse pups were treated with carbonyl iron (cat. no. C3518, Sigma Aldrich) in three different dosages (60, 120, or 240 mg/kg body weight) dissolved in 5% sorbitol (cat. no. S1876, Sigma Aldrich) in H_2O via oral gavage between postnatal days 10 and 17, as previously described (Carboni et al., 2017). The control group was treated with vehicle only. To avoid injuries, special feeding tubes for mouse pups were used for the gavage (cat. no. FTP22-25, Instech Laboratories).

Stereotactic injections of 12-week-old mice were conducted as described previously (Saal et al., 2015; Tatenhorst et al., 2014). The animals received an analgesic treatment with Metamizole (1.5 mg/ml) in drinking water, starting 2 days before surgery and ending 2 days after the injection of α-syn. Mice were anesthetized by intraperitoneal injection of ketamine (150 mg/kg body weight) and xylazine (10 mg/kg body weight) and fixed in a stereotactic frame. Eyes were protected by application of eye ointment. For all stereotaxic injection experiments, human-derived monomeric α-syn and α-syn PFFs were employed. Coordinates for intrastriatal injections into the right hemisphere were set relative to Bregma (anteroposterior axis: +0.4 mm, mediolateral axis: −1.8 mm, dorsoventral axis: −3.5 mm). After incision and trepanation, 2 μl of α-syn human monomer or PFFs solution (5 μg) was injected at an injection rate of 500 nl/min. The injection capillary was left in place for 4 min to prevent reflux, then slowly removed, and the incision was closed with tissue glue (cat. no. 129463, DermaBond, Ethicon). After surgery, mice were placed on a warming pad until wake up, and then returned to their home cage.

Motor behavior was analyzed using the rotarod test (cat. no. 47600, Ugo Basile) as previously described (Tatenhorst et al., 2016). Briefly, mice were placed on a rotating rod for 5 min with accelerating speed from 5 to 40 rpm. Up to five mice were tested simultaneously. Mice were pre-trained on two consecutive days before the first assessment to reach stability in rotarod performance. The test was conducted weekly, starting after stereotactic injections. All behavioral tests were performed in the afternoon. Each mouse performed three trials (5 min each) on the rotarod per test day with an intertrial interval of 30 min to reduce stress and fatigue. Per session, the time in seconds the mouse spent on the rod was recorded.

The novel object recognition (NOR) test to analyze short-term memory (STM) and long-term memory (LTM) was performed before α-syn PFFs injection and before killing (Bevins & Besheer, 2006; Tatenhorst et al., 2016). Each mouse was placed into an empty arena of 48 x 35 cm for 3 min to habituate. Next, two identical objects were placed inside the arena for 5 min to familiarize the mouse with the objects. After a 10-min recovery (STM testing condition), or after 24 hr (LTM condition), the respective mouse was placed again into the arena with one familiar and one novel object. The exploratory behavior of each mouse was videotaped for 5 min and afterwards analyzed with Ethovision XT 8.5 software (Noldus, Wageningen, The Netherlands). Based on the time spent with the novel object compared to the time spent with both objects, a discrimination ratio was calculated as previously described (Tatenhorst et al., 2016).

Animals were killed at 90 days post-α-syn injection (dpi). This time point was selected based on previous studies (Luk, Kehm,

Carroll, et al., 2012; Luk, Kehm, Zhang, et al., 2012), demonstrating a well-advanced spreading of α-syn fibrils through the brain at this stage. For perfusions, mice received a lethal intraperitoneal injection of ketamine (300 mg/kg body weight (bw)) and xylazine (15 mg/kg bw) solution. Under deep anesthesia, mice were then transcardially perfused with 50-ml ice-cold PBS within 5 min followed by 50 ml of 4% paraformaldehyde (PFA, cat. no. A3813, Applichem) at pH 7.4 within 5 min. The brains were post-fixed with 4% PFA in PBS for 24 hr at 4°C and afterwards transferred into 30% sucrose (cat. no. A2211, Applichem) in PBS for cryopreservation for 48 hr. Cryosections of 30-μm thickness were prepared on a cryostat (CM3060, Leica, Wetzlar, Germany) and either directly mounted on Superfrost slides (cat. no. J1800AMNZ, Menzel, Braunschweig, Germany) and frozen at −20°C, or stored free-floating in 24-well plates in PBS with 0.1% sodium azide (cat. no. A1430, Applichem) until usage for immunohistochemical staining.

2.3 | Primary cell culture preparation and treatment

C57Bl/6J donor mice of E18.5 embryos received a lethal intraperitoneal injection of ketamine (300 mg/kg bw) and xylazine (15 mg/kg bw) solution. After explantation, the embryos were decapitated, the brains were dissected, and the primary cortex neurons were prepared in ice-cold calcium–magnesium-free medium (1x HBSS, cat. no. 14180-046, Gibco, with 0.12% bicarbonate solution, cat. no. 25080-60, Gibco). Cells were incubated in 1-ml Trypsin (≥ 9,000 U/mg; 1.87 mg/ml; cat. no. T9935, Sigma Aldrich) for 12 min at 37°C. After adding DNAse (~400 U/mg; cat. no. DN25-100, Sigma Aldrich), the suspension was centrifuged and Trypsin/DNAse was replaced by 1-ml fetal calf serum (FCS; cat. no. S0615, Biochrom) to stop digestion. FCS was then substituted with cell culture medium (Neurobasal medium, cat. no. 21103-049, Gibco, containing holo-transferrin, cat. no. A3124, Applichem, PSN, cat. no. 15640-055, Gibco, L-Glutamine 200 mM, cat. no. 25030-024, Gibco, and B27 supplement 1:50, cat. no. 17504-044, Gibco) and 120,000 neurons were seeded in the primary cell compartment of a microfluidic chamber (cat. no. 855.234.0044, Xona). The other compartment was filled with medium. One day later, half of the medium was exchanged with cytosine arabinoside-containing medium (AraC; cat. no. C6645, Sigma Aldrich) to reach a concentration of 2 μM AraC. On day in vitro 2 (div 2), medium was changed to medium containing 100-μM $FeCl_2$ (stock solution 5 mM $FeCl_2$, cat. no. 372870, Sigma Aldrich, diluted in 5% glucose, cat. no. G8769, Sigma Aldrich). The control condition was treated with an equal amount of 5% glucose. After 24 hr, cells were washed twice with medium. Subsequently, the medium was changed to α-syn containing medium (1 μg in 200 ml medium). For all cell culture experiments, mouse-derived α-syn PFFs were employed. After 24 hr, cells were washed. On div 7, 250,000 cells (preparation on E 18.5) were seeded into the secondary cell compartment. Medium change was performed every second day. On div 14, cells were fixed with 4% PFA in PBS for 10 min and stored in PBS at 4°C.

2.4 | Quantification of ferric iron levels in the brain tissue of iron- and vehicle-treated mice

To analyze the levels of ferric iron in brain tissue of iron-treated and control mice, midbrain sections from animals that received a postnatal treatment with either vehicle (sorbitol) or 240 mg/kg Fe were mounted on object slides and immunostained with the Iron Stain Kit (Prussian Blue Stain Kit, cat. no. ab150674, Abcam). Stainings were performed following the manufacturer's instructions with small modifications. The incubation for the background staining (Nuclear FastRed, provided in the above mentioned kit) was reduced to 60 s after a 1:20 dilution. Quantitative analyses of iron-stained samples were imaged using the Mosaix module (AxioVision SE64 Rel. 4.8 software, Carl Zeiss) on a Zeiss Axioplan microscope using a 10x magnification. Iron-positive signals and background signals were selected using the iLastik software version 1.3.3 (Berg et al., 2019), followed by the generation of segmentation images for each section (contained only pixels for iron-positive regions). Segmentation micrographs were converted to 8-Bit, binarized and quantified using the ImageJ software (National Institute of Health, Bethesda, MD). Briefly using the ROI manager, the areas of substantia nigra (SN) pars compacta/pars reticulata, cortex, brainstem, and hippocampus were selected for each section based on the Paxinos mouse brain atlas (Paxinos & Franklin, 2003). The average pixel intensity was quantified for each selected region and normalized by the total selected area (in pixels). A schematic of the procedure is given in Figure S8a.

2.5 | X-ray fluorescence imaging

For X-ray fluorescence (XRF) analysis, we used 6-month-old female and male mice, which were neonatally enriched with 60 or 120 mg/kg body weight iron. Control mice were treated with vehicle only. After killing the mice, brains were explanted, the hemispheres were separated, and cut into 5-mm-thick sections. These single sections were mounted in cryo matrix (cat. no. 14020108926, Leica) and cryofixed for 2 min in 2-methyl-butane (cat. no. M32631, Honeywell) placed in liquid nitrogen to avoid ice crystal formation. Samples were stored in liquid nitrogen until further analysis. Frozen brain samples were cut into 30-μm sections on a CM3060 Leica Cryostat, freeze-dried, and mounted between two layers of 4-μm ultralene foil (cat. no. 3525, SpexSamplePrep) as described before (Vogel-Mikuš et al., 2014). XRF imaging of freeze-dried brain sections was performed at the XRF beamline of Synchrotron Elettra, Trieste (Karydas et al., 2018). The samples were positioned at an angle of 45° and scanned by 75 × 75 μm beam at excitation energy of 10 keV. XRF was detected by a silicon drift detector (SDD) (XFlash 5030, Bruker, Nano GmbH), which was placed on the incident beam horizontal plane, perpendicular to the primary beam. The SDD has a 30 mm^2 nominal crystal area, a thickness of 450 μm and nominal resolution equal to 131 eV (at Mn-K) (Karydas et al., 2018).

XRF spectra were fitted by PyMCA (Solé et al., 2007) and quantified as previously described (Kump & Vogel-Mikuš, 2018). The

XRF system was calibrated using pure metal foils (MicromatterTM Technologies Inc.) and validated using standard reference materials (cat. no. NIST1537a, Tomato Leaves, Sigma Aldrich). Sample thickness was determined using absorption that was detected by a photodiode placed behind the sample and scattering of X-rays on the sample (Kump & Vogel-Mikuš, 2018).

2.6 | Analysis of α-syn spreading pathology

To analyze α-syn spreading pathology within the mouse brain, sections mounted on object slides underwent antigen retrieval procedure in citrate buffer (cat. no. 5110.3, Roth, Karlsruhe, Germany; pH 6.0) at 80°C for 30 min. After cooling to 21°C and washing, sections were incubated for 20 min in 25-mM glycine (cat. no. A1377, Applichem) in PBS. Following the application of 0.1% Sudan black (cat. no. A1407, Applichem) for 15 min, sections were rinsed in water and washed in PBS. Sections were then incubated for 1.5 hr at 21°C in a blocking solution (10% normal horse serum, cat. no. SHD3250YK, Linaris, Mannheim, Germany, 5% bovine serum albumin (BSA; IgG free, cat. no. 001000162, Jackson ImmunoResearch), 0.3% TritonX, cat. no. A4975, Applichem, 25 mM glycine in PBS). The sections were incubated with rabbit anti-pS129 α-syn antibody (1:1,000; EP1536Y, cat. no. ab51253, Abcam) in blocking solution at 4°C overnight. After washing, sections were incubated with the secondary antibody (Cy3 goat anti-rabbit, 1:500, cat. no. 111-165-006, Dianova, Hamburg, Germany) for 1.5 hr at RT. After washing for 3 × 10 min, 4′,6-diamidino-2-phenylindole (DAPI, cat. no. A1001, Applichem) was applied for 2 min and after final washing, the sections were dried at 37°C for 10 min and embedded with Mowiol (cat. no. 0713.2, Sigma Aldrich).

For a quantitative analysis of pS129-α-syn signal, immunostained samples were imaged using the MosaiX module of AxioVision SE64 Rel. 4.9 software (Carl Zeiss) on a Zeiss Axioplan microscope. Representative exemplary photomicrographs are provided in Figure S2. Images of the Cy3 channel were converted to 8-bit and the threshold function of ImageJ (National Institute of Health) was used to manually adjust the threshold for every image. A schematic overview of the analysis procedure is given in Figure S3. The adjusted threshold of the greyscale was ranging from 231 to 250. It was verified that the manually adjusted threshold values did not differ significantly between images from different animals (Figure S4). Next, the corresponding image of the DAPI channel was used to calculate the area (in pixel^2) of the injected and the contralateral hemisphere separately as regions of interest (ROIs). pS129-α-syn-positive signal within ROIs was calculated by the 'analyze particles' tool of ImageJ. Results were given as percentages resulting from the signal area divided by the total area of the corresponding hemisphere.

To describe pS129-α-syn spreading to different brain regions, ImageJ was used to overlay the generated threshold image from quantification analysis with DAPI images showing the brain structures (Figure S3). Brain regions were adjusted according to the Paxinos mouse brain atlas (Paxinos & Franklin, 2003) and marked where the overlay images showed pS129-α-syn signal. In addition, the occurrence of pS129-α-syn signal was graded for each brain region using a five-stage scale (0–4) as follows: - no positive signal, + few (sporadic positive structures), ++ mild (several positive structures, but not widespread), +++ moderate (many positive structures covering a widespread part of the brain region), and ++++ severe (almost the whole brain region is covered with pS129-α-syn signal). Exemplary images per stage are illustrated in Figure S5. Six to eight animals were evaluated per group and a mean signal amount was calculated for each positively graded brain region. A color code was assigned to the stage-scaled graduation and the results were illustrated as heat maps. The Allen Mouse Brain Connectivity Atlas (©2020 Allen Institute for Brain Science. Allen Mouse Brain Connectivity Atlas, available from: https://connectivity.brain-map.org/) (Oh et al., 2014) was used to analyze pS129-α-syn spreading to anatomically connected regions. The connectivity platform contains data of different EGFP injection experiments and enables to follow the affected and connected brain regions starting from the injection site. Based on the selection of two injection experiments of the aforementioned platform (Exp. 158916311: https://connectivity.brain-map.org/projection/experiment/158916311 and Exp. 100142580: https://connectivity.brain-map.org/projection/experiment/100142580), of which the injection sites are located in the injection radius of our study, the anatomical connectivity of this study was reconstructed. Respective brain regions were illustrated in connectivity maps of the six selected brain sections for our analysis. In a final step, the six connectivity maps were compared with the pS129-α-syn spreading maps to visualize intersections.

For the in vitro experiment, fixed cells were incubated with 25-mM glycine in PBS for 20 min. After washing, cells were incubated with blocking solution for 1.5 hr at 21°C. Primary antibodies against α-syn fibrils (rabbit anti-α-syn pS129, 1:1,000, cat. no. EP1536Y; Abcam) and MAP2 (mouse anti-MAP2, 1:200, cat. no. MAB3418; Merck Millipore) were diluted in blocking solution and cells were incubated with the antibody solution overnight at 4°C. After washing and incubation with the secondary antibodies for 1.5 hr at 21°C (Cy3 goat anti-rabbit, 1:500, cat. no. 111-165-006, Dianova, Hamburg, Germany; Cy5 goat anti-mouse, cat. no. 111-175-146, Jackson ImmunoResearch), cells were washed and counter-stained with DAPI for 2 min. The cells were mounted with Mowiol and finally imaged on a Zeiss Axioplan microscope (magnification 200x; AxioVision SE64 Rel. 4.9 software; MosaiX module). pS129- α-syn signal was assessed using the threshold function of ImageJ as described above. Per culture (n = 5) one threshold was defined, which was used to analyze the chambers of the different conditions. The secondary cell compartment was defined as region of interest (ROI). A percentage was generated from the signal area and ROI area and, afterwards, the average of one to three chambers per condition was calculated. Using the PBS condition as control, the relative signal (%) of the PBS condition was subtracted from the relative signal (%) of the monomer or PFFs conditions, respectively.

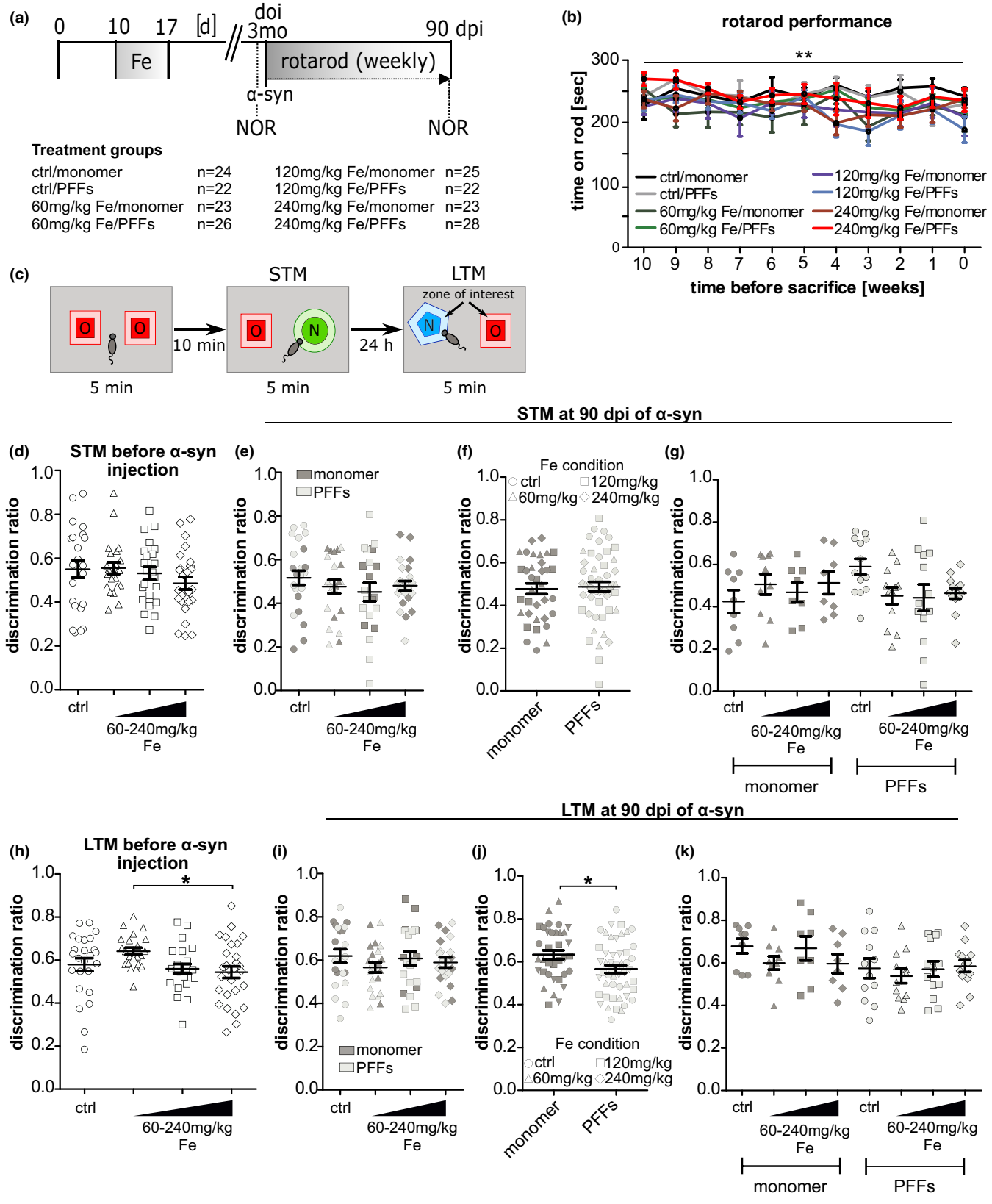

2.7 | Microglia and T-cell quantification

To investigate the immune cell response after α-syn PFF injections, microglia and T cells were analyzed in the brain tissue of mice. Immunohistochemical staining for CD11b+ microglia was performed using 30-μm PFA-fixed coronal cryosections of the substantia nigra (SN) and striatum. Free-floating sections were pre-incubated for 3 hr at 21°C on a shaker with 5% BSA/5% normal goat serum (NGS; cat. no. CL1200-100, Cedarlane Labs) in 0.01 M PBS before being incubated overnight at RT with the primary rat anti-mouse CD11b

antibody (1:100, cat. no. MCA74G, Bio-Rad Laboratories), diluted in 1% BSA/1% PBS in 0.01 M PBS. To visualize the CD11b primary antibody, sections were then incubated for 2 hr with biotinylated secondary antibody against rat Igs (1:100, cat. no. BA-9401-0.5, Vector Laboratories) diluted in 1% PBS/1% NGS in 0.01 M PBS followed by avidin/biotin reagent (cat. no. 32020, Thermo Fisher Scientific) before incubation and staining with diaminobenzidine-HCl (DAB) and H_2O_2 (DAB substrate kit, cat. no. SK-4100, Vector Laboratories). Cell nuclei were counter-stained with Hematoxylin (cat. no. T865.2, Carl Roth).

Quantification of CD11b+ microglia was performed with a light microscope (Olympus BH2, Olympus, Hamburg, Germany) using an ocular grid covering a defined area (0.0625 mm^2) at a final magnification of 400x. For each animal, the PFFs-injected and contralateral sides were investigated separately by quantifying on average two sections per region and two to three grids per section. The cell number of immune cells was then calculated per square millimeter.

Immunohistochemical stainings for CD3+ T cells were performed using 30-µm PFA-fixed coronal cryosections of the SN and striatum. Free-floating sections were pre-incubated for 3 hr at 21°C on a shaker with 5% BSA/5% NGS in 0.01 M PBS before being incubated for 2 hr at RT with the primary rat anti-mouse CD3 antibody conjugated with Alexa Fluor® 488 (1:50, cat. no. 100210, Biolegend). DAPI staining was performed to label cell nuclei.

Quantification of T-cell numbers was performed using a Zeiss Axio Imager.M2 fluorescence microscope. Because of the low number of T cells, the entire regions of the SN (pars compacta and pars reticulata), the pre-commissural, commissural, and post-commissural parts of the striatum were analyzed, respectively. The cell number of immune cells was then calculated per square millimeter.

2.8 | Statistical analysis

SPSS statistics 26.0 (IBM) and Graphpad Prism 5.04 (Graphpad Software) were used for statistical analyses. The Kolmogorov–Smirnov test was used to evaluate the normality of the data. The results indicated that when alpha =0.05, $p > .05$ confirmed that data were normally distributed. No test for outliers was conducted. Analysis of variance (ANOVA) with repeated measurements, one-way and two-way ANOVA, Kruskal–Wallis test, Fisher's exact test, two-tailed Student's *t* test, and Mann–Whitney U test were calculated as indicated. For multiple group comparisons, Tukey's post hoc tests or Dunn's post hoc test were used. Sample sizes of the experiments as well as used statistical tests are specified in the respective figure legends. All analyses were performed by a blinded investigator. Data are given as mean ± standard error of the mean (*SEM*). Differences were considered significant with $p < .05$ ($^*p < .05$; $^{**}p < .01$; $^{***}p < .001$).

3 | RESULTS

3.1 | Behavioral effects of iron treatment and injection of α-syn PFFs in mice

To investigate how iron treatment and α-syn PFFs injections influence motor and cognitive behavior, mice were tested on the rotarod and in the novel object recognition (NOR) test. Animals treated with different concentrations of iron (60, 120, or 240 mg/kg body weight) or sorbitol as vehicle and injected with α-syn monomer or PFFs performed the rotarod test weekly between the day of α-syn injection (doi) and killing (90 dpi). The NOR test was performed twice: directly before doi to investigate the effect of iron intoxication, and directly before killing to investigate combined effects of iron intoxication and α-syn PFFs injections (Figure 1a).

Analysis of the rotarod data revealed that iron and PFFs treatment did not affect the motor behavior (Figure 1b). Only for the variable "time before killingAccording to the style sheet, the word "sacrificed" should be avoided. Hence it has been changed to "killed" and "killing" according to the context. Please check.", ANOVA with repeated measures indicated that the average of all mice shows a slight continuous decline of the time spent on the rotarod ($^{**}p < .01$; overall mean 10 weeks: 241.0 ± 17.1 s versus overall mean at time of killing [0 weeks]: 223.3 ± 19.2 s).

The NOR test was used to test both short-term memory (STM) and long-term memory (LTM) by modifying the timeframe between habituation and recall phase (10 min versus 24 hr; Figure 1c). Before PFFs injection, high-dose iron-treated mice (0.49 ± 0.03) showed no significant difference in their STM as compared to controls

FIGURE 1 Experimental layout and evaluation of motor and cognitive behavior of mice treated with iron and α-syn monomer or preformed fibrils (PFFs). (a) Experimental layout of treatment and behavioral testing of C57Bl/6J mice. Numbers of mice for the respective treatment groups are indicated. No mice were excluded. (b) Results of the weekly performed rotarod test starting 10 weeks before killing. The averaged performance of mice per treatment group ($n = 6–8$ mice per group) over time is shown. The averaged performance of all mice changes significantly over time (main effect of variable "time", $^{**}p < .01$). Data given as mean ± *SEM*, ANOVA with repeated measures with Greenhouse–Geisser correction. (c) Experimental procedure of the novel object recognition (NOR) test. (d–g) Short-term memory (STM) results (d) before α-syn injection ($n = 21–22$ mice per group) and (e–g) at 90 days post-injection (dpi), displaying the main effects of the two single variables—(e) iron treatment and (f) α-syn injection. (g) shows combined effects of iron and α-syn treatments ($n = 8–13$ mice per group). (h–k) Long-term memory (LTM) results (h) before α-syn injection and (i–k) at 90 dpi, displaying the main effects of the treatment variables—(i) iron treatment and (j) α-syn injection. (k) shows the combined effects of iron and α-syn treatments ($n = 8–13$ mice per group). Fe-triangle indicates the three different treatment groups of low, middle, and high iron concentrations (60, 120, and 240 mg/kg Fe). Data given as mean ± *SEM*; $^*p < .05$, $^{**}p < .01$; One-way and two-way ANOVA with Tukey's post hoc test as well as Kruskal–Wallis test with Dunn's post hoc test

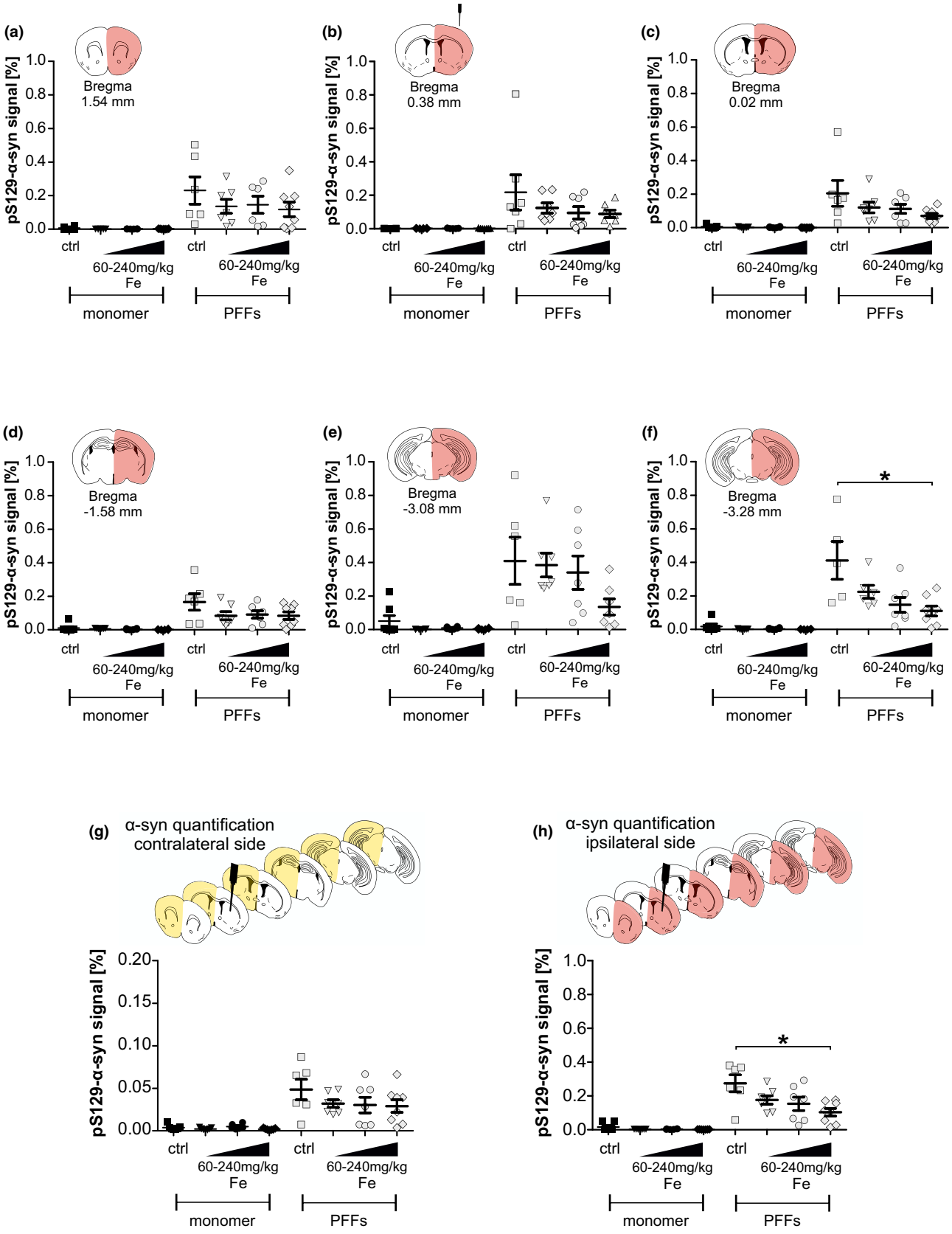

(0.54 ± 0.04; Figure 1d). Regarding the LTM at this time point (Figure 1h), mice treated with 240 mg/kg iron (0.54 ± 0.02) performed significantly worse in LTM compared to mice of the 60 mg/kg iron group (0.64 ± 0.02; $^*p < .05$), but not compared to controls (0.58 ± 0.03). At 90 dpi, neither an interaction effect of iron×α-syn on STM nor a main effect of the separate treatment conditions (iron

or α-syn treatment) could be detected (Figure 1e–g). Focusing on LTM, the interaction effect of iron×α-syn was not significant and no main differences between the iron-treatment groups were found. However, two-way ANOVA revealed a significant main effect of α-syn injections showing moderately reduced discrimination ratios in LTM for PFFs-injected mice (0.63 ± 0.02 vs. 0.56 ± 0.02; Figure 1i–k; $^{*}p < .05$).

As a control variable of general mobility, the distance moved within the NOR arena was analyzed for both time points (Figure S6). Before α-syn PFFs or monomer injection, no significant differences of mice treated with different iron concentrations were observed when compared to controls. Only mice of the 240 mg/kg iron group (1,286 ± 67 cm) showed a decreased distance moved compared to both the 120 mg/kg iron group (1622 ± 113 cm; $^{*}p < .05$) and the 60 mg/kg iron group (1715 ± 79 cm; $^{**}p < .01$) at 24 hr post-habituation phase. However, none of these groups was significantly different when compared to controls (1,472 ± 87 cm). At 90 dpi, no significant differences in movement were detected between the treatment groups.

3.2 | Analysis of iron in tissue from iron-treated animals

Synchrotron micro-XRF analyses of freeze-dried SN sections as well as Prussian blue iron stainings of cryosections from 6-month-old mice were performed to verify increased brain iron in C57Bl/6J mice treated with carbonyl iron between postnatal days 10 and 17. In XRF analyses, quantitative iron distribution maps were generated after scanning SN sections with a 75-μm beam and an average iron value was extracted from the region of the SN of mice treated with 60 mg/kg Fe (25 and 31.2 μg/g), 120 mg/kg Fe (25.4 and 40.6 μg/g), or vehicle (7.1 and 4.4 μg/g) as indicated (Figure S7a, b). Mice treated with iron showed at least threefold increase of iron concentration within the SN compared to control mice (Figure S7c). A significant increase of iron was also confirmed by Prussian blue iron staining in the SN (vehicle: 0.006 ± 0.001 normalized average pixel intensity versus 240 mg/kg Fe: 0.010 ± 0.004 normalized average pixel intensity, Figure S8b) as well as in the cortex (vehicle: 0.031 ± 0.008 normalized average pixel intensity versus. 240 mg/kg Fe: 0.065 ± 0.033 normalized average pixel intensity, Figure S8c), and in the hippocampus (vehicle: 0.010 ± 0.002 normalized average pixel intensity versus. 240 mg/kg Fe: 0.017 ± 0.004 normalized average pixel intensity, Figure S8e). No significant difference could be detected in the brainstem (vehicle: 0.004 ± 0.002 normalized average pixel intensity versus. 240 mg/kg Fe: 0.006 ± 0.001 normalized average pixel intensity, Figure S8d).

3.3 | Quantification of α-syn spreading pathology in vivo

To assess the influence of iron on the spreading of α-syn pathology induced by the seeding of PFFs, we performed a threshold-based quantification of phosphorylated (pS129) α-syn. This post-translationally-modified subtype of α-syn has been reported to enhance its toxicity both in vivo and in vitro, as well as to increase the formation of α-syn aggregates (Chen et al., 2009; Fujiwara et al., 2002; Smith, 2005). Six coronal mouse brain sections named after their coordinates relative to Bregma were analyzed and the pS129-α-syn signal was normalized to the area of the region of interest and compared between the treatment groups. As expected, virtually no pS129-α-syn signal could be detected in the α-syn monomer-injected animals, independent of iron dosage (Figure 2).

At 90 days following α-syn PFFs injection, pS129-α-syn signal was detected in all six analyzed brain sections (Figure 2a–f). Interestingly, in the injected hemisphere, the five most rostral sections (Bregma +1.54, +0.38, +0.02, −1.58, and −3.08 mm, Figure 2a–e) did not show any significant difference in pS129-α-syn signal after iron treatment, although the control-treated group always showed numerically more pS129-α-syn signal as compared to the iron-treated groups. However, the most caudal section that also contained the SN (Bregma −3.28, Figure 2f) displayed a significantly decreased pS129-α-syn signal after high-dose iron treatment (240 mg/kg iron: 0.11 ± 0.03% vs. ctrl: 0.41 ± 0.11%; $^{*}p < .05$).

Furthermore, we calculated the pS129-α-syn signal average of all available brain sections per mouse separately for signal in the contralateral (Figure 2g) and ipsilateral hemisphere (Figure 2h). At the contralateral hemisphere, the overall pS129-α-syn signal of PFFs-injected animals was markedly lower as compared to the injected hemisphere. No significant difference between groups was observed here. In the PFFs-injected hemisphere, mice showed significantly

FIGURE 2 Quantification of pS129-α-syn signal in the mouse brain. At 90 days post-injection (dpi), brain sections immunostained with a pS129-α-syn antibody were analyzed with the particle analysis tool of the ImageJ software. All sections were selected based on the Paxinos mouse brain atlas (Paxinos & Franklin, 2003). (a–f) The data points within the scatter plots represent the pS129-α-syn signal of each mouse per group. The sections correspond to (a) Bregma +1.54 mm (n = 5–8), (b) Bregma +0.38 mm as the injectional plane (n = 5–7 mice per group), (c) Bregma +0.02 mm (n = 6–8 mice per group), (d) Bregma −1.58 mm (n = 6–8 mice per group), (e) Bregma −3.08 mm (n = 6–7 mice per group), and (f) Bregma −3.28 mm (n = 5–8 mice per group). (g, h) The averaged pS129-α-syn signal per mouse individually per each hemisphere: (g) contralateral hemisphere and (h) injected hemisphere. Average of the brain sections mentioned above (four to six available sections per animal). Each data point within the scatter plots represents the pS129-α-syn signal of one mouse per group (n = 6–8 mice per group). Iron triangle indicates the three different treatment groups of low, middle, and high iron dosage (60, 120 and 240 mg/kg Fe). Data are shown as mean ± *SEM*; statistical comparison of the four preformed fibrils (PFFs) groups with Kruskal–Wallis test with Dunn's post hoc test; $^{*}p < .05$

higher pS129-α-syn signal in the 240 mg/kg iron-treated group (0.10 ± 0.02%; *$p < .05$) as compared to controls (0.27 ± 0.05%).

3.4 | Iron-dependent changes in α-syn spreading pathology in different brain areas

In order to analyze whether iron treatment changed the α-syn spreading pathology in PFF-injected mouse brains, brain sections were stained for pS129-α-syn. Spreading maps were generated for selected brain sections, similar to previously published analyses (Luk, Kehm, Carroll, et al., 2012; Masuda-Suzukake et al., 2013, 2014; Paumier et al., 2015). The spreading of α-syn pathology to different brain regions was quantified in six coronal brain sections and illustrated in heat maps to compare the pS129-α-syn spreading pattern between PFFs-injected mice treated with vehicle and high dosage iron (240 mg/kg).

As shown in Figure 3a, the overall α-syn spreading pattern between iron- and vehicle-treated mice was largely similar. In Tables S1–S6, all brain regions exhibiting α-syn pathology and the according semi-quantified pathology ratings are summarized corresponding to the six evaluated coronal brain sections. Between iron-treated and control animals, distinct differences in the quantity of pS129-α-syn aggregates within specific brain regions were found, which are visualized in specific subtraction heat maps (Figure 3b).

Here, in the injected hemisphere, the most prominent difference (at least two levels, e.g., + versus. +++) was observed within the cingulate cortex area 1, the primary motor cortex, perirhinal cortex, lateral amygdaloid nucleus, stria terminalis, and the amygdalohippocampal area. In all of these brain regions, the control group showed an increased pS129-α-syn signal compared to the iron group. Iron-treated mice showed more pS129-α-syn signal (two-level difference) at the contralateral hemisphere within the agranular insular area. Mostly, group differences showed only one rating level of distance such as – versus +or + versus ++. The quantification of regions showing a higher α-syn amount in either iron-treated or vehicle-treated mice is summarized in a fourfold table in Figure 3c. For the injected hemisphere, a higher number of regions with more α-syn signal was found in the PFFs-injected group with vehicle treatment as compared to iron-treated animals (*$p < .05$, Fisher's exact test).

3.5 | Connectivity analysis

Based on the Allen Mouse Brain Connectivity Atlas (©2020 Allen Institute for Brain Science. Allen Mouse Brain Connectivity Atlas, available from https://connectivity.brain-map.org/) (Oh et al., 2014), pS129-α-syn spreading to anatomically connected brain regions and brain regions beyond the connectome was analyzed based on the data presented in Figure 3.

In iron-treated, but also in vehicle-treated mice with PFFs injection, the pS129-α-syn spreading signal was observed in brain regions of the connectome but also in other brain regions (Figure 4a–c). By adding up all pS129- α-syn-positive brain regions out of the six evaluated brain sections and dividing these regions into both connectome-based/connectome-independent brain regions, a fourfold table was designed to indicate that, in vehicle-treated mice, more connectome-associated brain regions were affected than in iron-treated mice. On the other hand, iron-treated mice show more connectome-independent brain areas affected (Figure 4d). In the following analysis, we aimed to assess which of the mouse groups (iron- or vehicle-treated) showed more pS129-α-syn staining, in connectome-specific brain regions or connectome-independent brain regions (Figure 4e–f), in order to investigate the influence of iron on connectivity-based pS129-α-syn-spreading. Therefore, pS129-α-syn rating averages of all affected brain regions (six evaluated brain sections) were considered and grouped for iron- and vehicle-treated animals. The graphs show the data for each of these groups individually. The average of these ratings of different brain regions was compared between both groups. Whereas vehicle-treated mice showed significantly higher α-syn pathology levels in affected connectome-specific brain regions (ctrl: 0.99 ± 0.09 vs. Fe: 0.70.± 0.07; *$p < .05$, Mann–Whitney U test, Figure 4e), in connectome-independent brain regions no significant group differences were found (ctrl: 0.64 ± 0.05 versus. Fe: 0.47 ± 0.03; Figure 4f).

3.6 | Microglia and T-cell distribution in the striatum of iron- and α-syn PFFs-treated mice

To analyze if microglial and/or T-cell activation contributes to the iron-mediated changes in pS129-α-syn distribution following PFFs injection, microglia were quantified in the striatum (Figure S9a–c). Figure 5c shows an exemplary image of CD11b+ microglia, which were quantified in this analysis.

In the injected hemisphere, the average of microglia cell numbers of three striatal sections resulted in a significantly increased microglia accumulation in vehicle/PFFs mice (333.5 ± 13.1 microglia/mm^2) compared to the monomer-injected mice (vehicle/monomer: 258.2 ± 13.6 microglia/mm^2 vs. 240 mg/kg Fe/monomer: 267.8 ± 15.5 microglia/mm^2). Whereas no significant difference was observed between the vehicle/PFFs group and the 60 mg/kg Fe/PFFs group (277.5 ± 19.8 microglia/mm^2), the vehicle/PFFs showed significantly increased microglia numbers compared to the 120 (254.1 ± 17.1 microglia/mm^2) and 240 mg/kg Fe/PFFs groups (238.9 ± 11.1 microglia/mm^2; Figure 5a). Furthermore, the injected hemisphere of one SN section was analyzed but no significant microglia differences were found between the groups (Figure S9d). In the contralateral hemisphere (Figure 5b), the vehicle/PFFs group (288.6 ± 10.5 microglia/mm^2) showed a significantly increased microglia accumulation compared to the 60 (230.0 ± 12.3

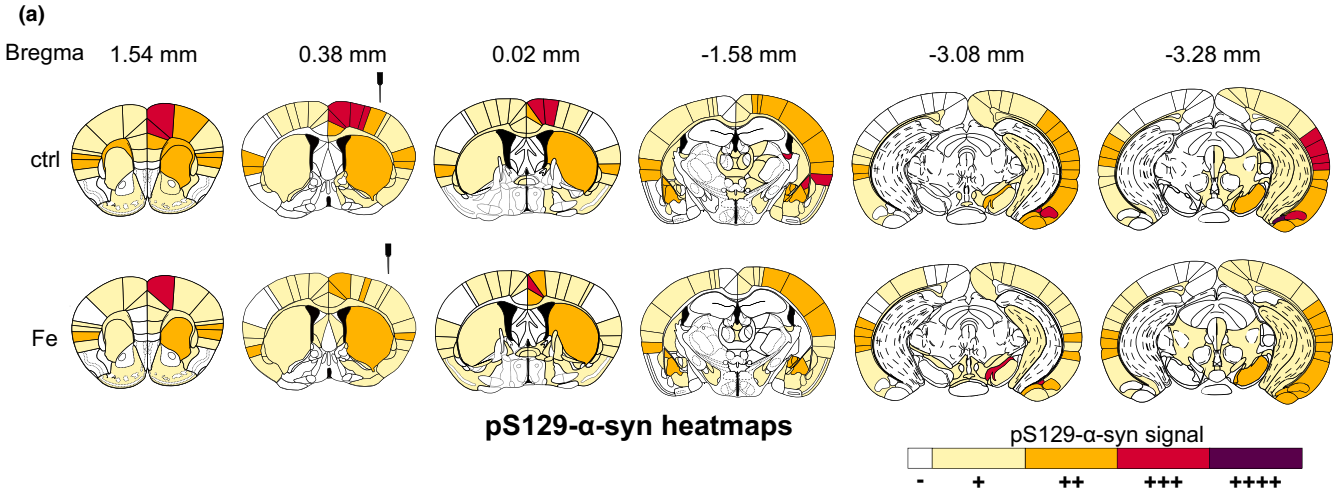

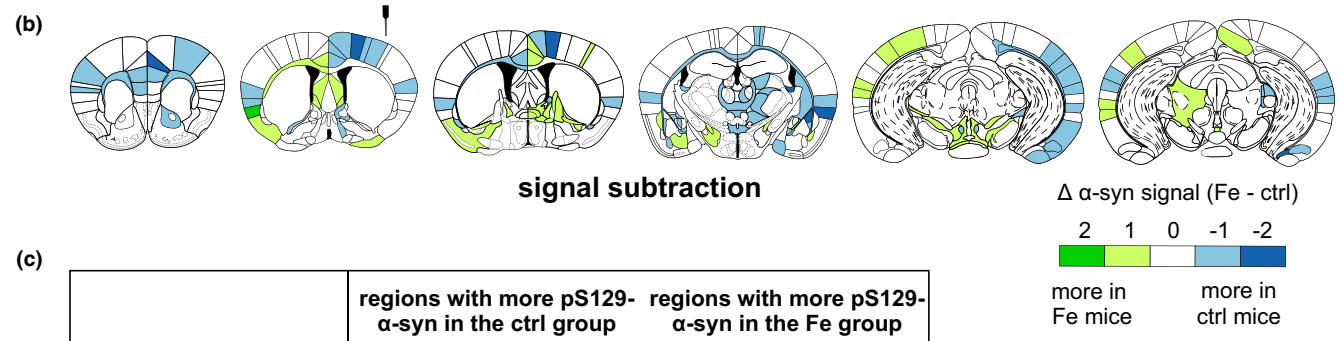

(c)

	regions with more pS129-α-syn in the ctrl group	regions with more pS129-α-syn in the Fe group
injected hemisphere	60*	25
contralateral hemisphere	26	26

FIGURE 3 Heat maps representing the distribution of pS129-α-syn in the brain of preformed fibrils (PFFs)-injected mice. (a) At 90 dpi, pS129-α-syn pathology was detected in PFFs-injected mice, which received previously a postnatal treatment with vehicle as control or 240 mg/kg Fe. The occurrence of pS129-α-syn in brain regions was graded with a five-stage scale (0–4), simplified as follows: "–" no positive structures, "+" few (sporadic positive structures), "++" mild (several positive structures but not widespread), "+++" moderate (many positive structures covering a widespread part of the brain region), and "++++" severe (almost the whole brain region is covered with pS129-α-syn signal). The average per treatment group for each brain region was calculated ($n = 6$–8 mice per group) and a color code was assigned to the scale. (b) Subtraction heat maps of the data shown in (a). The signal ratings of the control group were subtracted from the signal ratings of the iron group. 0 represents an equal signal in both groups and is represented in white color. Green color represents more α-syn pathology for iron-treated mice, whereas a blue color represents more pathology for vehicle-treated mice. (c) Fourfold table demonstrating significantly higher number of regions with more α-syn pathology in the control group compared to the iron-treated group in the injected hemisphere (*$p < .05$, Fisher's exact test)

microglia/mm^2) and 240 mg/kg Fe/PFFs groups (226.2 ± 11.6 microglia/mm^2). PFFs-injected mice treated with 120 mg/kg Fe showed unaltered microglia counts (242.7 ± 14.2 microglia/mm^2). In addition, the vehicle/PFFs group exhibited an increased microglia accumulation compared to the vehicle/monomer group (237.4 ± 11.5 microglia/mm^2). In the SN, no significant differences in microglia numbers were found between the groups (Figure S9e).

To assess a potential contribution of T cells to α-syn spreading, brain sections were additionally immunolabeled for CD3. However, our data showed no significant differences in T-cell counts between groups, neither in striatal nor in SN sections (Figure S10).

3.7 | Contribution of iron to spreading of α-syn PFFs in vitro

After showing that iron treatment attenuated α-syn spreading throughout the brain of C57Bl/6J mice, we wanted to assess if this effect could also be observed in an in vitro PFFs spreading assay in microfluidic chambers. Primary murine cortex neurons were used to investigate if iron influences PFFs spreading in glia-free conditions. First, the cell toxicity of different iron dosages was assessed (Figure S11). Based on previously optimized $FeCl_2$ concentrations in cell culture models (Dai et al., 2013; Oexle et al., 1999; Solntseva et al., 2015), iron treatment was performed at a concentration of

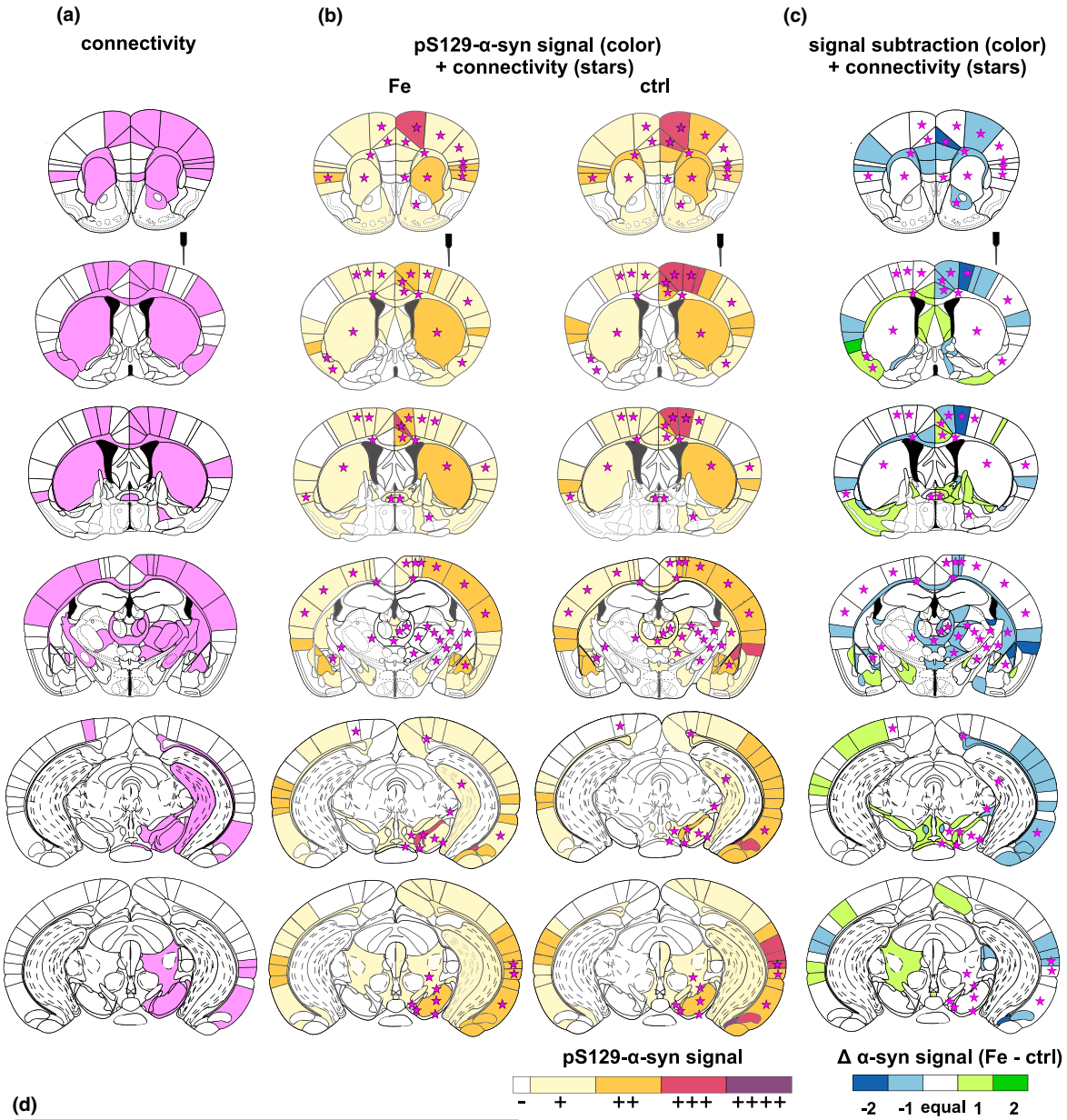

(d)

	Fe group	ctrl group
connectome-specific brain areas with pS129-α-syn signal	66	75
connectome-independent brain areas with pS129-α-syn signal	166	155

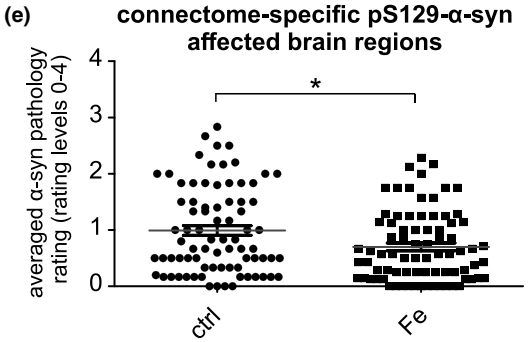

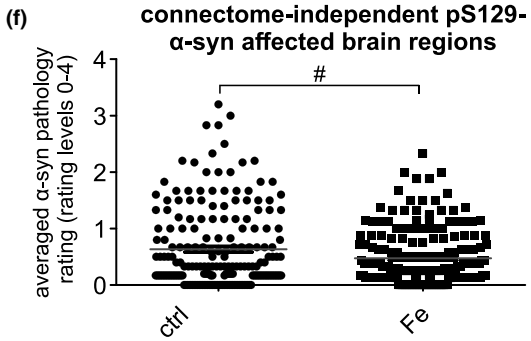

100-μM $FeCl_2$, where no toxic effects were observed. Neurons were treated with either $FeCl_2$ or vehicle at div2 for 24 hr and afterwards for 24 hr with α-syn PFFs or monomers (Figure 6a).

Figure 6b displays an exemplary photomicrograph of cells immunostained with an antibody recognizing pS129-α-syn showing that α-syn pathology was transmitted to cells of the secondary cell compartment. pS129-α-syn signal within the secondary cell compartment was quantified in all different conditions (PBS, monomer or PFFs; with or without $FeCl_2$) and normalized to the respective PBS-only treated control condition (Figure 6c). In the secondary cell compartment, significantly more pS129-α-syn signal was detected in the PFFs-treated cells as compared to monomer-treated cells, but no influence of $FeCl_2$ treatment was observed in this model ($FeCl_2$/PFFs 0.015 ± 0.0048 vs. vehicle/PFFs 0.013 ± 0.0042). Figure S12 demonstrates that pS129-α-syn signal was present only intracellularly but not extracellularly.

4 | DISCUSSION

Iron accumulation and α-syn aggregation are histopathological hallmarks of PD. However, it remains still unknown if both mechanisms synergistically affect each other, or whether they contribute to PD pathogenesis independently. In vitro experiments could already show that iron can bind to α-syn (Binolfi et al., 2006; Davies et al., 2011; Peng et al., 2010) and is able to foster α-syn aggregation (Golts et al., 2002; Kostka et al., 2008; Uversky et al., 2001). Therefore, we postulated that iron enrichment occurring in particular areas of PD brains (Dexter et al., 1991) may also affect α-syn spreading pathology.

In order to model increased iron levels in the mouse brain, we administered carbonyl iron via oral gavage to mice at neonatal days 10–17. In this period, the blood–brain barrier is known to be still open for iron (Billings et al., 2016, 2019; McCarthy & Kosman, 2008). As expected, we confirmed increased iron levels in adult mice by XRF analysis and Prussian blue iron staining of brain tissue. PFFs injections were performed at 12 weeks of age, and mice were analyzed at 90 dpi with regard to α-syn spreading pathology. This schedule was selected, since a well-advanced α-syn spreading pathology in the brain after PFFs injection has been previously reported at this time point (Luk, Kehm, Carroll, et al., 2012; Luk, Kehm, Zhang, et al., 2012).

With regard to motor behavior, our experiments pointed out that neither PFFs nor iron treatment did affect the rotarod performance of mice. These results are in line with former studies treating rodents with either iron or α-syn species (Carboni et al., 2017; Chen et al., 2015; Luk, Kehm, Carroll, et al., 2012). Previous studies investigating memory function after iron supplementation in rodents, however, showed a significant cognitive decline (Fredriksson et al., 2000; de Lima, Laranja, et al., 2005; de Lima, Polydoro, et al., 2005; de Lima et al., 2007; Schröder et al., 2001). Here, we analyzed STM and LTM at two-time points: before α-syn PFFs injection and at 90 dpi. Whereas iron treatment did not have any effect on STM and LTM before α-syn PFFs injection in our study, only LTM was impaired at 90 dpi, regardless of iron dosage. These findings are, in part, contradictory to previous studies showing a significant LTM decline after iron treatment at p12–14, but also no effects on STM at 3 months of age (de Lima et al., 2007). Another study in rats showed that STM was only affected when iron was applied between postnatal days 19–21 (de Lima, Polydoro, et al., 2005). We, thus, hypothesize that neonatal brain iron enrichment is dependent on the species as well as on the time point of iron application. Interestingly, we observed a moderately impaired LTM, which was independent of overall movement after intrastriatal seeding of PFFs. A previous study showed that spatial and working memory were affected when α-syn over-expression was combined with intrastriatal α-syn PFFs injections (Espa et al., 2019). In addition, pS129-α-syn signal within brain regions relevant to memory formation could also contribute to PFFs-dependent memory dysfunction in our study. Perirhinal and insular cortices were described to be essential for the consolidation of familiar objects (Balderas et al., 2008; Bermudez-Rattoni et al., 2005). In LTM, but not in STM, the ventromedial prefrontal cortex (infralimbic and prelimbic cortex) was highly involved in the consolidation and reconsolidation of object recognition memory (Akirav & Maroun, 2006) and these regions were also affected in our model. Although it was shown that LTM of object recognition is dependent on hippocampal integrity (Clarke et al., 2010), the hippocampus was only rarely affected in our model. Object details and spatial locations in STM were found to be carried within the entorhinal cortex (Suzuki et al., 1997). Although we detected pS129-α-syn signal within the entorhinal cortex, no deficits in STM could be observed. Here, unaffected brain regions possibly compensated for the dysfunction of affected areas.

FIGURE 4 pS129-α-syn pathology in connectome-specific and connectome-independent brain regions. (a) Connectivity maps of six coronal brain sections were generated based on two experiments (Exp. 158916311; Exp. 100142580) of the Allen Brain Connectivity Atlas (©2020 Allen Institute for Brain Science. Available from: https://connectivity.brain-map.org/). (b) pS129-α-syn pathology maps as shown in Figure 3. Anatomically connected brain regions according to (a) are highlighted by pink asterisks. (c) Heat maps of signal subtraction as shown in Figure 3 combined with stars indicating anatomically connected brain regions according to (a). (d) Fourfold table of the quantity of connectome-specific and connectome-independent brain regions that are affected by α-syn pathology. (e and f) Averaged pS129-α-syn ratings in connectome-specific and connectome-independent brain regions. Brain regions were included as soon as at least one of both treatment groups showed α-syn pathology. The graphs are related to the data in (b). The averaged α-syn pathology ratings in either (e) anatomically connected ($n = 78$ brain areas) or (f) connectome-independent brain regions ($n = 198$ brain regions) were compared between iron- and vehicle-treated mice. Mann–Whitney *U* test. Mean ± *SEM*; $^*p < .05$; $\#p < .1$

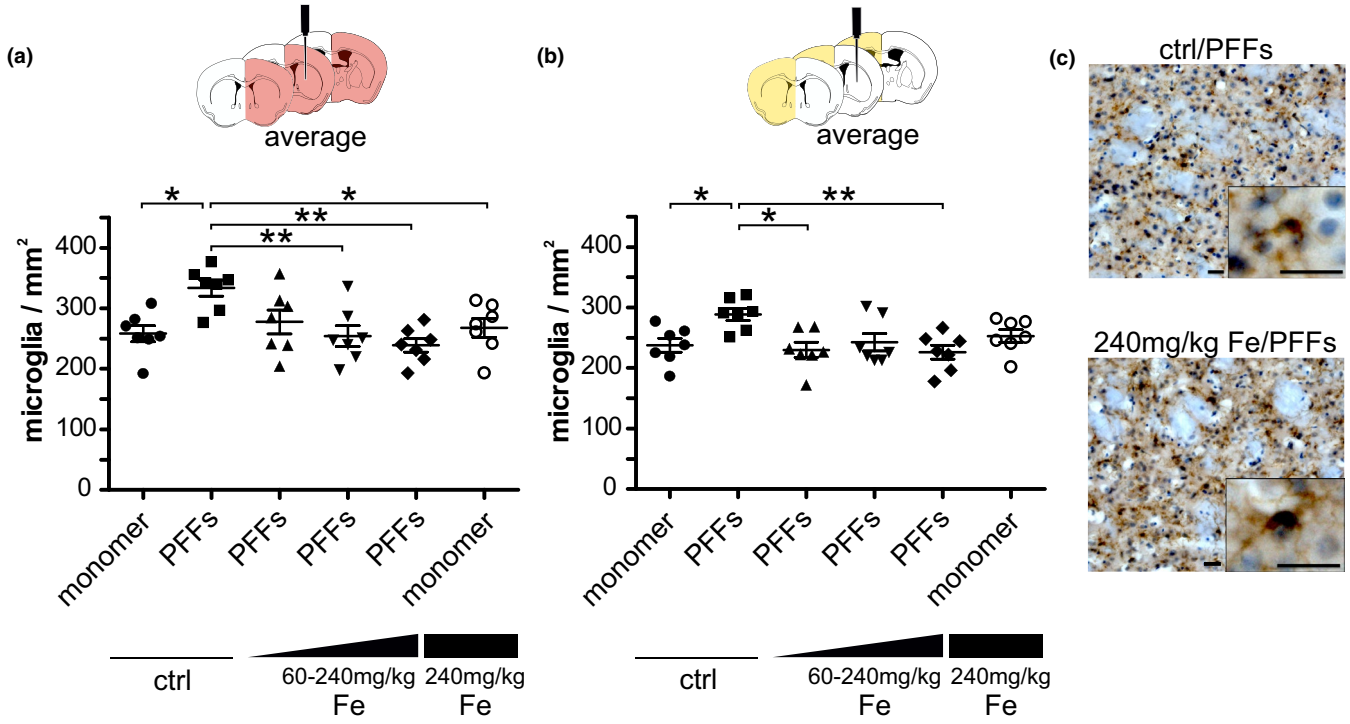

FIGURE 5 Microglia analysis in the striatum of iron- and preformed fibrils (PFFs)-treated mice. Brain sections were immunostained with an antibody recognizing CD11b. (a) Averaged microglia numbers within the striatum (average of 1–3 sections) at the injected hemisphere (all groups $n = 7$ mice per group). (b) Averaged microglia numbers within the striatum (average of sections) at the contralateral hemisphere (all groups $n = 7$ mice per group). (c) Exemplary images of immunostained CD11b-positive cells from mice treated with vehicle or 240 mg/kg Fe (with the close-up image in the right corner of each image). Scale bar is 20 μm. Iron triangle indicates the three iron dosages (60, 120, and 240 mg/kg Fe) and control indicates the vehicle control. Data given as mean ± *SEM*, one-way ANOVA with Tukey's post hoc test; $^{*}p < .05$, $^{**}p < .01$

Advanced α-syn spreading pathology can be observed at 90 dpi and is dependent on the amount of injected PFFs and on the genotype of the used animals (Blumenstock et al., 2017; Kim et al., 2016; Luk, Kehm, Carroll, et al., 2012; Luk, Kehm, Zhang, et al., 2012; Shimozawa et al., 2017; Terada et al., 2018). To better understand the hypothesized contribution of iron to the propagation of α-syn pathology, we determined whether pS129-α-syn spreading was altered after neonatal brain iron enrichment. Brain regions showing pS129-α-syn pathology in our model largely overlapped with areas affected in similar studies using intrastriatal PFFs injections in wild-type mice, but differed with regard to injection sites (Chung et al., 2019). The spreading pattern of pS129-α-syn pathology in our study was similar to the study of Luk and colleagues, demonstrating pS129-α-syn signal, e.g., in cortical regions, amygdaloid nuclei, SN, and within the amygdalopiriform transition area (Luk, Kehm, Zhang, et al., 2012).

Contrary to our expectations, we observed that the amount of the applied carbonyl iron was reciprocal to the detected pS129-α-syn signal. According to the pS129-α-syn spreading maps, the affected brain regions were mostly similar in control- and iron-enriched animals, but differed markedly in the detected aggregate amount. Iron-enriched mice showed significantly less α-syn pathology in connectome-specific regions. Studies in PD patients underscore this finding, where an increased intrastriatal iron content led to a reduced functional cross-talk between the striatum and distant brain areas of other resting-state networks (Salami et al., 2018). A further study with PD patients suggested a negative correlation of nigral iron content and the functional connectivity (Guan et al., 2019), supporting the hypothesis that iron altered the connectivity in our model, thereby influencing α-syn spreading pathology. Another study performing PFFs injections into the dorsal striatum highlighted α-syn spreading to anatomically connected brain regions and identified the basolateral amygdala, rostral cortical regions, and the piriform cortex as the most vulnerable regions for α-syn spreading (Henderson et al., 2019). Our data showed that α-syn spreading pathology affected connectome-specific and connectome-independent regions. Strikingly, not all anatomical connections were involved in α-syn spreading pathology and the ones affected displayed unequal amounts of pS129-α-syn signal. It was suggested that the number of neuronal projections between regions and the projection length could influence the vulnerability of regions, presuming that anatomical connectivity is an influencing factor but does not exclusively determine the spreading pathology of α-syn (Oliveira et al. 2019).

Since elevated levels of iron may lead to increased oxidative stress in brain tissue, we further analyzed the possible iron-mediated induction of neuroimmunological responses, which could further influence α-syn spreading pathology. Therefore, the number of microglia cells in the brain was quantified. PFFs-injected control mice showed a significant increase in striatal microglia, which was absent in iron-enriched animals.

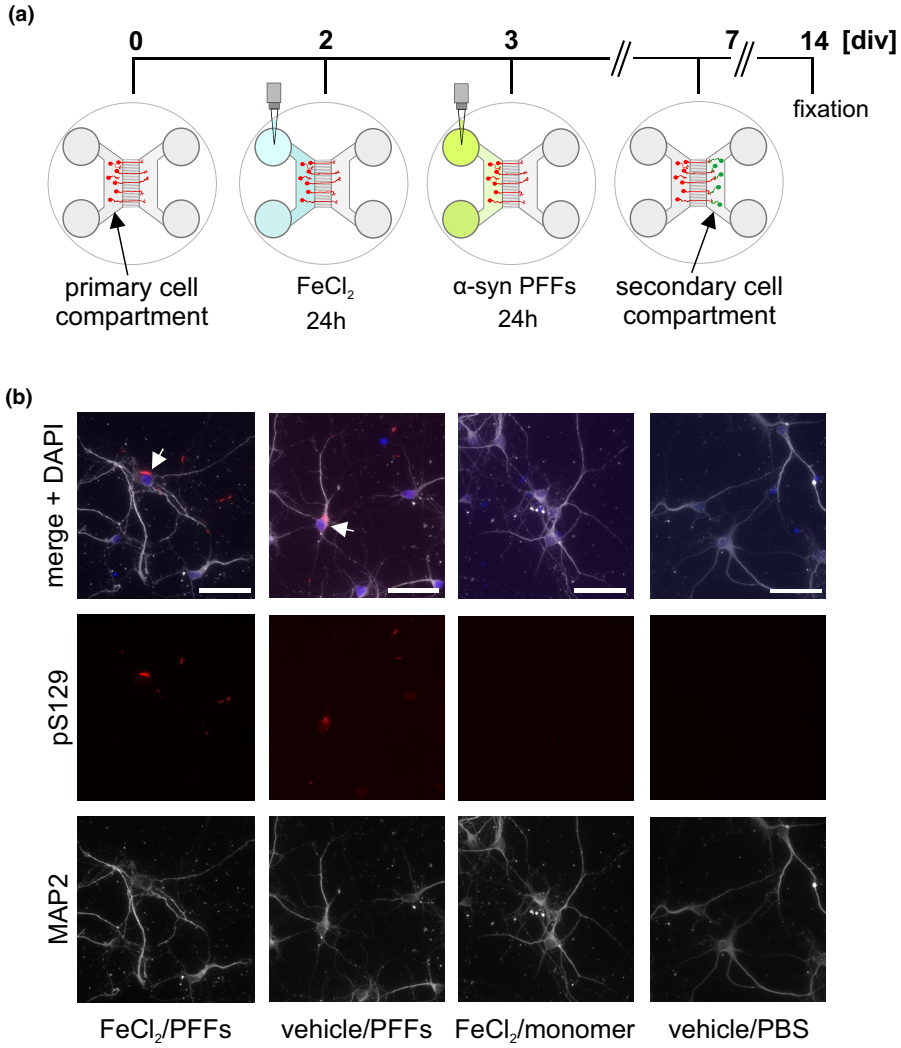

FIGURE 6 Quantification of pS129-α-syn signal in vitro. (a) Layout of the microfluidic chamber culture experiment of primary neurons treated with $FeCl_2$ and α-syn preformed fibrils (PFFs). (b) Exemplary photomicrographs of α-syn PFFs-treated neurons in the secondary compartment of a microfluidic chamber. Cells were immunolabeled for α-syn fibrils (pS129). White arrows point to pS129-α-syn-positive neurons. Scale bar is 20 μm. (c) Quantification of the area of pS129-α-syn signal within the secondary compartment of microfluidic chambers which was normalized to the total area of this compartment and is, therefore, giving as percentage (average of 1–3 chambers per culture, $n = 5$ cultures, each data point within the scatter plot represents one culture). pS129-α-syn signal of all conditions was normalized to the respective PBS control. Kruskal–Wallis test with three selected Dunn's post hoc comparisons. $^*p < .05$; ns, not significant

It is known that α-syn species that are released by neurons into the extracellular space can activate microglia and foster α-syn-mediated microglial migration (Kim et al., 2013; Lee et al., 2010; Zhang et al., 2005). This migration process depends on the binding of α-syn to the cell adhesion molecule Integrin α-*M* (CD11b) (Wang et al., 2015). Furthermore, microglia density strongly correlated with the density of α-syn molecules (Peelaerts et al., 2015). In line with this, our data confirm that PFFs trigger microglial activation and recruitment. However, it remains still unclear which role microglia play after their migration to the injection site. Even if microglia are major scavenger cells of α-syn aggregates, clearance mechanisms are rather unlikely due to the conformational state of α-syn (Lee et al., 2008). This explanation is confirmed by other studies in which highly ordered aggregates were found to interfere with the phagocytic ability of microglia (Choi et al., 2015; Park et al., 2008). Furthermore, a recent study reported stronger α-syn spreading pathology to intrastriatally grafted dopaminergic neurons in mice after microglia activation (George et al., 2019), and microglia was recently also attributed a role as an α-syn transporter in vitro (Valdinocci et al., 2018). Therefore, our results may support the hypothesis that microglia rather facilitate α-syn spreading pathology. Since traveling microglia do not necessarily follow axonal anatomical networks, this could explain why α-syn pathology could be found in many regions not associated with the connectome in our model. It has also been demonstrated that the exosome-related α-syn transmission can be supported by microglia (Xia et al., 2019). On these grounds, we propose that the injected α-syn PFFs induced activation and migration of microglia which may possibly contribute to α-syn spreading pathology.

The presence of T cells in the striatum and SN was analyzed, since it is known from mouse models of PD that T cells infiltrate the brain and especially the SN (Brochard et al., 2009; González et al., 2013). Against the expectations, no significant intergroup differences in T-cell amounts within the striatum or the SN could be observed. In a study by Harms and colleagues, short α-syn fibrils were not only able to activate and recruit microglia but also peripheral cells as monocytes, macrophages, and lymphocytes (Harms et al., 2017). Specifically, 8 weeks post-α-syn PFFs injection into the SN of rats, a significant infiltration with T cells as well as monocytes/macrophages was observed within the SN. However, microglia amounts did not increase within the injection site (Harms et al., 2017). In comparison with this study, Harms and colleagues used a higher α-syn dosage (8 μg), a different injection site (SN), different animal species (rats), and an earlier time point of analysis (8 weeks post-injection). Especially the latter could explain the different output in our study. Probably the acute immune response of T cells occurred earlier, and the analysis time point in our study was, therefore, too late to detect an infiltration (Joppe, 2020, https://d-nb.info/1211816877/34).

Subsequent to the analysis of the impact of iron on α-syn spreading pathology in vivo, an in vitro experiment was performed to elucidate the effect of iron on pS129-α-syn spreading after seeding of α-syn PFFs in cortical neurons. Using the microfluidic chamber model, cells treated with iron and PFFs showed unaltered pS129-α-syn spreading from the primary to the secondary cell compartment. In the past, microfluidic chamber models were commonly used to analyze anterograde and retrograde α-syn fibrils transmission as well as axonal transport and transmission to second-order neurons (Freundt et al., 2012; Tran et al., 2014; Volpicelli-Daley et al., 2011), identifying microfluidic chambers as a practicable device to analyze spreading of α-syn. However, iron possibly affects different transmission mechanisms of α-syn which cannot be depicted with this setup, especially the involvement of other, non-neuronal cell types. This may be further supported by a recent report that found that PFFs did not cause iron-dependent ferroptosis (Guiney et al., 2020).

Clearly, our study has limitations: Our models use exogenous administration of PFFs, which can only indirectly be transferred to α-syn spreading pathology in human PD patients, since the amount and isoform of PFFs as well as the age of the mice were shown to influence the outcome (Blumenstock et al., 2017; Kim et al., 2016; Luk, Kehm, Carroll, et al., 2012; Luk, Kehm, Zhang, et al., 2012; Shimozawa et al., 2017; Terada et al., 2018). Age is the major risk factor of PD (Milanese et al., 2018), and also directly affects dopamine metabolism (Adolfsson et al., 1979) and brain iron content (Loeffler et al., 1995), making future studies with aged mice advisable. α-syn was shown to be entangled in iron transport and dysregulated iron homeostasis promoting iron-dependent ferroptosis (Baksi et al., 2016). Furthermore, iron can enhance formation and recruitment of α-syn oligomers, by that enabling redox cycling and oxidative catalysis of lipids and dopamine metabolites (Duce et al., 2017). Therefore, the additional use of iron chelators appears as a promising therapeutic strategy (Finkelstein et al., 2016). The disease-modifying effects of the iron-chelator Deferiprone were already investigated in clinical trials in PD patients (Devos et al., 2014; ClinicalTrials.gov. National Library of Medicine (U.S.) 2015; Martin-Bastida et al., 2017). However, iron chelation therapy is challenging and requires a fine-tuned iron equilibrium in blood and tissue to avoid unwanted adverse effects (Cabantchik et al., 2013; Devos et al., 2014; Moreau et al. 2018).

To conclude, our study demonstrated a PFFs-induced cognitive decline in mice, a reduction of microglia in the striatal PFFs injection site, as well as an iron-mediated modulation of the α-syn aggregate pathology in the mouse brain. Iron-enriched mice showed a reduction of pS129-α-syn spreading pathology, suggesting that iron-dependent alterations of the brain connectome may lead to a redistribution of α-syn aggregates in the brain. The reduction of striatal microglia mediated by iron in PFFs-injected mice warrants further studies analyzing the role of non-neuronal cells in α-syn spreading pathology.

ACKNOWLEDGMENTS

The authors thank Sabine Ceramella, Vivian Dambeck, Elisabeth Barski, and Karin Giller for expert technical assistance and Carmina Warth Perez Arias for assistance in sample delivery. We acknowledge equipment support by the laboratory of Prof. Tiago Outeiro. The Facility for Electron Microscopy at MPI-BPC, Goettingen, is acknowledged for imaging of PFFs. Elettra Synchrotron Trieste is acknowledged for the provision of the beamtime (Project 20175078). Giuliana Aquilanti is acknowledged for the help with the beamline alignment and measurements. Relevant content presented in this article has been published

as part of the thesis entitled "Alpha-synuclein spreading pathology in Parkinson's disease: the influence of iron and the Rho-kinase inhibitor fasudil." authored by Karina Joppe at the Georg-August-University Goettingen, Germany (https://d-nb.info/1211816877/34). This work was supported by the Deutsche Forschungsgemeinschaft (DFG, German Research Foundation) under Germany's Excellence Strategy—EXC 2067/1- 390729940, as well as by the Max Planck Society. P.L. received funding from the Cluster of Excellence and DFG Research Center Nanoscale Microscopy and Molecular Physiology of the Brain (CNMPB), Goettingen and a Physics-to-Medicine seed grant of the University Medical Center Goettingen. All data generated or analyzed during this study are included in this published article and its supplementary information files.

All experiments were conducted in compliance with the ARRIVE guidelines.

FUNDING STATEMENT

Open Access funding enabled and organized by Projekt DEAL.WOA Institution: GEORG-AUGUST-UNIVERSITAET GOTTINGENBlended DEAL: Projekt DEAL

CONFLICT OF INTEREST

Mathias Bähr is a former Senior Editor of the Journal of Neurochemistry. The authors declare that they have no conflict of interests.

AUTHOR CONTRIBUTIONS

KD, LT, LCG, MB, KV-M, CWI, MZ, and PL planned and designed the experiments. KD, LT, LCG, SZ, MP, EC, A-ER, HED, KV-M, and SB performed the experiments. KD, LT, LCG, and PL performed statistical analyses of the study and interpreted the data. PL supervised the study. KD, LT, LCG, and PL wrote the manuscript.

OPEN RESEARCH BADGES

This article has received a badge for Open Materials because it provided all relevant information to reproduce the study in the manuscript. More information about the Open Science badges can be found at https://www.cos.io/initiatives/badges.

DATA AVAILABILITY STATEMENT

Data available in article supplementary material.

ORCID

Lars Tatenhorst https://orcid.org/0000-0002-6690-688X
Lucas Caldi Gomes https://orcid.org/0000-0003-4959-2169
Mojan Parvaz https://orcid.org/0000-0002-0644-5559
Paul Lingor https://orcid.org/0000-0001-9362-7096

REFERENCES

Adolfsson, R., Gottfries, C. G., Roos, B. E., & Winblad, B. (1979). Post-mortem distribution of dopamine and homovanillic acid in human brain, variations related to age, and a review of the literature. *Journal of Neural Transmission*, 45, 81–105. https://doi.org/10.1007/BF01250085

Akirav, I., & Maroun, M. (2006). Ventromedial prefrontal cortex is obligatory for consolidation and reconsolidation of object recognition memory. *Cerebral Cortex*, 16, 1759–1765. https://doi.org/10.1093/cercor/bhj114

Baksi, S., Tripathi, A. K., & Singh, N. (2016). Alpha-synuclein modulates retinal iron homeostasis by facilitating the uptake of transferrin-bound iron: Implications for visual manifestations of Parkinson's disease. *Free Radical Biology and Medicine*, 97, 292–306. https://doi.org/10.1016/j.freeradbiomed.2016.06.025

Balderas, I., Rodriguez-Ortiz, C. J., Salgado-Tonda, P., Chavez-Hurtado, J., McGaugh, J. L., & Bermudez-Rattoni, F. (2008). The consolidation of object and context recognition memory involve different regions of the temporal lobe. *Cold Spring Harbor Laboratory Press*, 15, 618–624. https://doi.org/10.1101/lm.1028008

Berg, D., Marek, K., Ross, G. W., & Poewe, W. (2012). Defining at-risk populations for Parkinson's disease: Lessons from ongoing studies. *Movement Disorders*, 27, 656–665. https://doi.org/10.1002/mds.24985

Berg, S., Kutra, D., Kroeger, T., Straehle, C. N., Kausler, B. X., Haubold, C., Schiegg, M., Ales, J., Beier, T., Rudy, M., Eren, K., Cervantes, J. I., Xu, B., Beuttenmueller, F., Wolny, A., Zhang, C., Koethe, U., Hamprecht, F. A., & Kreshuk, A. (2019). ilastik: Interactive machine learning for (bio)image analysis. *Nature Methods*, 16, 1226–1232. https://doi.org/10.1038/s41592-019-0582-9

Bermudez-Rattoni, F., Okuda, S., Roozendaal, B., & McGaugh, J. L. (2005). Insular cortex is involved in consolidation of object recognition memory. *Learning and Memory*, 12, 447–449. https://doi.org/10.1101/lm.97605

Bevins, R. A., & Besheer, J. (2006). Object recognition in rats and mice: A one-trial non-matching-to-sample learning task to study "recognition memory". *Nature Protocols*, 1, 1306. https://doi.org/10.1038/nprot.2006.205

Billings, J. L., Gordon, S. L., Rawling, T., Doble, P. A., Bush, A. I., Adlard, P. A., Finkelstein, D. I., & Hare, D. J. (2019). l-3,4-dihydroxyphenylalanine (l-DOPA) modulates brain iron, dopaminergic neurodegeneration and motor dysfunction in iron overload and mutant alpha-synuclein mouse models of Parkinson's disease. *Journal of Neurochemistry*, 150, 88–106.

Billings, J. L., Hare, D. J., Nurjono, M., Volitakis, I., Cherny, R. A., Bush, A. I., Adlard, P. A., & Finkelstein, D. I. (2016). Effects of neonatal iron feeding and chronic clioquinol administration on the parkinsonian human A53T transgenic mouse. *ACS Chemical Neuroscience*, 7, 360–366. https://doi.org/10.1021/acschemneuro.5b00305

Binolfi, A., Rasia, R. M., Bertoncini, C. W., Ceolin, M., Zweckstetter, M., Griesinger, C., Jovin, T. M., & Fernández, C. O. (2006). Interaction of α-synuclein with divalent metal ions reveals key differences: A link between structure, binding specificity and fibrillation enhancement. *Journal of the American Chemical Society*, 128, 9893–9901. https://doi.org/10.1021/ja0618649

Blumenstock, S., Rodrigues, E. F., Peters, F., Blazquez-Llorca, L., Schmidt, F., Giese, A., & Herms, J. (2017). Seeding and transgenic overexpression of alpha-synuclein triggers dendritic spine pathology in the neocortex. *EMBO Molecular Medicine*, 9, 716–731. https://doi.org/10.15252/emmm.201607305

Braak, H., Tredici, K., Del, R. U., de Vos, R. A. I., Jansen, S. E., & Braak, E. (2003). Staging of brain pathology related to sporadic Parkinson's disease. *Neurobiology of Aging*, 24, 197–211. https://doi.org/10.1016/S0197-4580(02)00065-9

Brochard, V., Combadière, B., Prigent, A., Laouar, Y., Perrin, A., Beray-Berthat, V., Bonduelle, O., Alvarez-Fischer, D., Callebert, J., Launay, J.-M., Duyckaerts, C., Flavell, R. A., Hirsch ,E. C., & Hunot, S. (2008). Infiltration of CD4+ lymphocytes into the brain contributes to neurodegeneration in a mouse model of Parkinson disease. *Journal*

of Clinical Investigation, 119, 182–192. https://doi.org/10.1172/jci36470

Burke, R. E., & O´Malley, K. (2014). Axon degeneration in Parkinson's disease. *Experimental Neurology*, 246, 72–83.

Cabantchik, Z. I., Munnich, A., Youdim, M. B., & Devos, D. (2013). Regional siderosis: a new challenge for iron chelation therapy. *Frontiers in Pharmacology*, 4, 1–7. https://doi.org/10.3389/fphar.2013.00167

Carboni, E., Tatenhorst, L., Tönges, L., Barski, E., Dambeck, V., Bähr, M., & Lingor, P. (2017). Deferiprone rescues behavioral deficits induced by mild iron exposure in a mouse model of alpha-synuclein aggregation. *NeuroMolecular Medicine*, 19, 309–321. https://doi.org/10.1007/s12017-017-8447-9

Chen, H., Wang, X., Wang, M., Yang, L., Yan, Z., Zhang, Y., & Liu, Z. (2015). Behavioral and neurochemical deficits in aging rats with increased neonatal iron intake: Silibinin's neuroprotection by maintaining redox balance. *Frontiers in Aging Neuroscience*, 7, 206. https://doi.org/10.3389/fnagi.2015.00206

Chen, L., Periquet, M., Wang, X., Negro, A., McLean, P. J., Hyman, B. T., & Feany, M. B. (2009). Tyrosine and serine phosphorylation of α-synuclein have opposing effects on neurotoxicity and soluble oligomer formation. *Journal of Clinical Investigation*, 119, 3257–3265. https://doi.org/10.1172/JCI39088

Choi, Y. R., Kang, S. J., Kim, J. M., Lee, S. J., Jou, I., Joe, E. H., & Park, S. M. (2015). FcγRIIB mediates the inhibitory effect of aggregated α-synuclein on microglial phagocytosis. *Neurobiology of Disease*, 83, 90–99. https://doi.org/10.1016/j.nbd.2015.08.025

Chung, H. K., Ho, H.-A., Pérez-Acuña, D., & Lee, S.-J. (2019). Modeling α-synuclein propagation with preformed fibril injections. *Journal of Movement Disorders*, 12, 139–151. https://doi.org/10.14802/jmd.19046

Clarke, J. R., Cammarota, M., Gruart, A., Izquierdo, I., & Delgado-García, J. M. (2010). Plastic modifications induced by object recognition memory processing. *Proceedings of the National Academy of Sciences of the United States of America*, 107, 2652–2657. https://doi.org/10.1073/pnas.0915059107

ClinicalTrials.gov. National Library of Medicine (U.S.) (2015) Conservative Iron Chelation as a Disease-modifying Strategy in Parkinson's Disease (FAIRPARKII). *European Multicentre, Parallel-group, Placebo-controlled, Randomized Clinical Trial of Deferiprone. (Identifier: NCT02655315)*.

Dai, M., Zhong, Z., Sun, Y., Sun, Q., Wang, Y., Yang, G., & Bian, L. (2013). Curcumin protects against iron induced neurotoxicity in primary cortical neurons by attenuating necroptosis. *Neuroscience Letters*, 536, 41–46. https://doi.org/10.1016/j.neulet.2013.01.007

Davies, P., Moualla, D., & Brown, D. R. (2011). Alpha-synuclein is a cellular ferrireductase. *PLoS One*, 6, e15814. https://doi.org/10.1371/journal.pone.0015814

de Lima, M. N. M., Laranja, D. C., Caldana, F., Grazziotin, M. M., Garcia, V. A., Dal-Pizzol, F., Bromberg, E., & Schröder, N. (2005). Selegiline protects against recognition memory impairment induced by neonatal iron treatment. *Experimental Neurology*, 196, 177–183. https://doi.org/10.1016/j.expneurol.2005.07.017

de Lima, M. N. M., Polydoro, M., Laranja, D. C., Bonatto, F., Bromberg, E., Moreira, J. C. F., Dal-Pizzol, F., & Schröder, N. (2005). Recognition memory impairment and brain oxidative stress induced by postnatal iron administration. *European Journal of Neuroscience*, 21, 2521–2528. https://doi.org/10.1111/j.1460-9568.2005.04083.x

de Lima, M. N. M., Presti-Torres, J., Caldana, F., Grazziotin, M. M., Scalco, F. S., Guimarães, M. R., Bromberg, E., Franke, S. I. R., Henriques, J. A. P., & Schröder, N. (2007). Desferoxamine reverses neonatal iron-induced recognition memory impairment in rats. *European Journal of Pharmacology*, 570, 111–114. https://doi.org/10.1016/j.ejphar.2007.06.002

Devos, D., Moreau, C., Devedjian, J. C., Kluza, J., Petrault, M., Laloux, C., Jonneaux, A., Ryckewaert, G., Garçon, G., Rouaix, N., Duhamel, A., Jissendi, P., Dujardin, K., Auger, F., Ravasi, L., Hopes, L., Grolez, G., Firdaus, W., Sablonnière, B., … Bordet, R. (2014). Targeting chelatable iron as a therapeutic modality in Parkinson's disease. *Antioxidants & Redox Signaling*, 21, 195–210. https://doi.org/10.1089/ars.2013.5593

Dexter, D. T., Carayon, A., Javoy-Agid, F., Agid, Y., Wells, F. R., Daniel, S. E., Lees, A. J., Jenner, P., & Marsden, C. D. (1991). Alterations in the levels of iron, ferritin and other trace metals in Parkinson's disease and other neurodegenerative diseases affecting the basal ganglia. *Brain*, 114, 1953–1975. https://doi.org/10.1093/brain/114.4.1953

Duce, J. A., Wong, B. X., Durham, H., Devedjian, J.-C., Smith, D. P., & Devos, D. (2017). Post translational changes to α-synuclein control iron and dopamine trafficking; a concept for neuron vulnerability in Parkinson's disease. *Molecular Neurodegeneration*, 12, 45. https://doi.org/10.1186/s13024-017-0186-8

Espa, E., Clemensson, E. K. H., Luk, K. C., Heuer, A., Björklund, T., & Cenci, M. A. (2019). Seeding of protein aggregation causes cognitive impairment in rat model of cortical synucleinopathy. *Movement Disorders*, 34(11), 1–12. https://doi.org/10.1002/mds.27810

Faul, F., Erdfelder, E., Buchner, A., & Lang, A.-G. (2009). Statistical power analyses using G*Power 3.1: Tests for correlation and regression analyses. *Behavior Research Methods*, 41, 1149–1160. https://doi.org/10.3758/BRM.41.4.1149

Finkelstein, D. I., Hare, D. J., Billings, J. L., Sedjahtera, A., Nurjono, M., Arthofer, E., George, S., Culvenor, J. G., Bush, A. I., & Adlard, P. A. (2016). Clioquinol improves cognitive, motor function, and microanatomy of the alpha-synuclein hA53T transgenic mice. *ACS Chem Neurosci*, 7, 119–129. https://doi.org/10.1021/acschemneuro.5b00253

Fredriksson, A., Schröder, N., Eriksson, P., Izquierdo, I., & Archer, T. (2000). Maze learning and motor activity deficits in adult mice induced by iron exposure during a critical postnatal period. *Developmental Brain Research*, 119, 65–74. https://doi.org/10.1016/S0165-3806(99)00160-1

Freundt, E. C., Maynard, N., Clancy, E. K., Roy, S., Bousset, L., Sourigues, Y., Covert, M., Melki, R., Kirkegaard, K., & Brahic, M. (2012). Neuron-to-neuron transmission of α-synuclein fibrils through axonal transport. *Annals of Neurology*, 72, 517–524. https://doi.org/10.1002/ana.23747

Fujiwara, H., Hasegawa, M., Dohmae, N., Kawashima, A., Masliah, E., Goldberg, M. S., Shen, J., Takio, K., & Iwatsubo, T. (2002). α-Synuclein is phosphorylated in synucleinopathy lesions. *Nature Cell Biology*, 4, 160–164. https://doi.org/10.1038/ncb748

George, S., Rey, N. L., Tyson, T., Esquibel, C., Meyerdirk, L., Schulz, E., Pierce, S., Burmeister, A. R., Madaj, Z., Steiner, J. A., Escobar Galvis, M. L., Brundin, L., & Brundin, P. (2019). Microglia affect α-synuclein cell-to-cell transfer in a mouse model of Parkinson's disease. *Molecular Neurodegeneration*, 14, 1–22. https://doi.org/10.1186/s13024-019-0335-3

Golts, N., Snyder, H., Frasier, M., Theisler, C., Choi, P., & Wolozin, B. (2002). Magnesium inhibits spontaneous and iron-induced aggregation of α-synuclein. *Journal of Biological Chemistry*, 277, 16116–16123. https://doi.org/10.1074/jbc.M107866200

González, H., Contreras, F., Prado, C., Elgueta, D., Franz, D., Bernales, S., & Pacheco, R. (2013). Dopamine receptor D3 expressed on CD4+ T cells favors neurodegeneration of dopaminergic neurons during Parkinson's disease. *The Journal of Immunology*, 190, 5048–5056.

Guan, X., Zhang, Y., Wei, H., Guo, T., Zeng, Q., Zhou, C., Wang, J., Gao, T., Xuan, M., Gu, Q., Xu, X., Huang, P., Pu, J., Zhang, B., Liu, C., & Zhang, M. (2019). Iron-related nigral degeneration influences functional topology mediated by striatal dysfunction in Parkinson's disease. *Neurobiology of Aging*, 75, 83–97. https://doi.org/10.1016/j.neurobiolaging.2018.11.013

Guiney, S. J., Adlard, P. A., Lei, P., Mawal, C. H., Bush, A. I., Finkelstein, D. I., & Ayton, S. (2020). Fibrillar α-synuclein toxicity depends on functional lysosomes. *Journal of Biological Chemistry*, 295, 17497–17513. https://doi.org/10.1074/jbc.RA120.013428

Harms, A. S., Delic, V., Thome, A. D., Bryant, N., Liu, Z., Chandra, S., Jurkuvenaite, A., & West, A. B. (2017). α-Synuclein fibrils recruit peripheral immune cells in the rat brain prior to neurodegeneration. *Acta Neuropathologica Communications*, 5, 85. https://doi.org/10.1186/s40478-017-0494-9

Henderson, M. X., Cornblath, E. J., Darwich, A., Zhang, B., Brown, H., Gathagan, R. J., Sandler, R. M., Bassett, D. S., Trojanowski, J. Q., & Lee, V. M. Y. (2019). Spread of α-synuclein pathology through the brain connectome is modulated by selective vulnerability and predicted by network analysis. *Nature Neuroscience*, 22, 1248–1257. https://doi.org/10.1038/s41593-019-0457-5

Hoyer, W., Antony, T., Cherny, D., Heim, G., Jovin, T. M., & Subramaniam, V. (2002). Dependence of α-synuclein aggregate morphology on solution conditions. *Journal of Molecular Biology*, 322, 383–393. https://doi.org/10.1016/S0022-2836(02)00775-1

Hoyer, W., Cherny, D., Subramaniam, V., & Jovin, T. M. (2004). Impact of the acidic C-terminal region comprising amino acids 109–140 on α-synuclein aggregation in vitro. *Biochemistry*, 43, 16233–16242.

Joppe, K. (2020). Alpha-synuclein spreading pathology in Parkinson's disease: The influence of iron and the Rho-kinase inhibitor fasudil. Germany: of the Georg-August-University Goettingen. Dissertation for the award of the degree "*Doctor rerum naturalium*"

Joppe, K., Roser, A.-E., Maass, F., & Lingor, P. (2019). The contribution of iron to protein aggregation disorders in the central nervous system. *Frontiers in Neuroscience*, 13, 15. https://doi.org/10.3389/fnins.2019.00015

Karydas, A. G., Czyzycki, M., Leani, J. J., Migliori, A., Osan, J., Bogovac, M., Wrobel, P., Vakula, N., Padilla-Alvarez, R., Menk, R. H., Gol, M. G., Antonelli, M., Tiwari, M. K., Caliri, C., Vogel-Mikuš, K., Darby, I., & Kaiser, R. B. (2018). An IAEA multi-technique X-ray spectrometry endstation at Elettra Sincrotrone Trieste: Benchmarking results and interdisciplinary applications. *Journal of Synchrotron Radiation*, 25, 189–203. https://doi.org/10.1107/S1600577517016332

Kim, C., Ho, D.-H., Suk, J.-E., You, S., Michael, S., Kang, J., Joong Lee, S., Masliah, E., Hwang, D., Lee, H.-J., & Lee, S.-J. (2013). Neuron-released oligomeric α-synuclein is an endogenous agonist of TLR2 for paracrine activation of microglia. *Nature Communications*, 4, 1562. https://doi.org/10.1038/ncomms2534

Kim, C., Lv, G., Lee, J. S., Jung, B. C., Masuda-Suzukake, M., Hong, C.-S., Valera, E., Lee, H.-J., Paik, S. R., Hasegawa, M., Masliah, E., Eliezer, D., & Lee, S.-J. (2016). Exposure to bacterial endotoxin generates a distinct strain of α-synuclein fibril. *Scientific Reports*, 6, 1–12. https://doi.org/10.1038/srep30891

Kostka, M., Högen, T., Danzer, K. M., Levin, J., Habeck, M., Wirth, A., Wagner, R., Glabe, C. G., Finger, S., Heinzelmann, U., Garidel, P., Duan, W., Ross, C. A., Kretzschmar, H., & Giese, A. (2008). Single particle characterization of iron-induced pore-forming α-synuclein oligomers. *Journal of Biological Chemistry*, 283, 10992–11003. https://doi.org/10.1074/jbc.M709634200

Kump, P., & Vogel-Mikuš, K. (2018). Quantification of 2D elemental distribution maps of intermediate-thick biological sections by low energy synchrotron μ-X-ray fluorescence spectrometry. *Journal of Instrumentation*, 13, C05014. https://doi.org/10.1088/1748-0221/13/05/C05014

Lee, E.-J., Woo, M.-S., Moon, P.-G., Baek, M.-C., Choi, I.-Y., Kim, W.-K., Junn, E., & Kim, H.-S. (2010). α-synuclein activates microglia by inducing the expressions of matrix metalloproteinases and the subsequent activation of protease-activated receptor-1. *The Journal of Immunology*, 185, 615–623. https://doi.org/10.4049/jimmunol.0903480

Lee, H. J., Suk, J. E., Bae, E. J., & Lee, S. J. (2008). Clearance and deposition of extracellular α-synuclein aggregates in microglia. *Biochemical and Biophysical Research Communications*, 372, 423–428. https://doi.org/10.1016/j.bbrc.2008.05.045

Loeffler, D. A., Connor, J. R., Juneau, P. L., Snyder, B. S., Kanaley, L., DeMaggio, A. J., Nguyen, H., Brickman, C. M., & LeWitt, P. A. (1995). Transferrin and iron in normal, Alzheimer's disease, and Parkinson's disease brain regions. *Journal of Neurochemistry*, 65, 710–716. https://doi.org/10.1046/j.1471-4159.1995.65020710.x

Luk, K. C., Kehm, V., Carroll, J., Zhang, B., Brien, P. O., Trojanowski, J. Q., & Lee, V. M. (2012). Pathological a-synuclein transmission initiates parkinson-like neurodegeneration in nontransgenic mice. *Science*, 338, 949–954.

Luk, K. C., Kehm, V. M., Zhang, B., O'Brien, P., Trojanowski, J. Q., & Lee, V. M. Y. (2012). Intracerebral inoculation of pathological α-synuclein initiates a rapidly progressive neurodegenerative α-synucleinopathy in mice. *Journal of Experimental Medicine*, 209, 975–986. https://doi.org/10.1084/jem.20112457

Martin-Bastida, A., Ward, R. J., Newbould, R., Piccini, P., Sharp, D., Kabba, C., Patel, M. C., Spino, M., Connelly, J., Tricta, F., Crichton, R. R., & Dexter, D. T. (2017). Brain iron chelation by deferiprone in a phase 2 randomised double-blinded placebo controlled clinical trial in Parkinson's disease. *Scientific Reports*, 7, 1398. https://doi.org/10.1038/s41598-017-01402-2

Masuda-Suzukake, M., Nonaka, T., Hosokawa, M., Kubo, M., Shimozawa, A., Akiyama, H., & Hasegawa, M. (2014). Pathological alpha-synuclein propagates through neural networks. *Acta Neuropathologica Communications*, 2, 88. https://doi.org/10.1186/s40478-014-0088-8

Masuda-Suzukake, M., Nonaka, T., Hosokawa, M., Oikawa, T., Arai, T., Akiyama, H., Mann, D. M. A., & Hasegawa, M. (2013). Prion-like spreading of pathological α-synuclein in brain. *Brain*, 136, 1128–1138. https://doi.org/10.1093/brain/awt037

McCarthy, R. C., & Kosman, D. J. (2008). Iron transport across the blood-brain barrier; Development, neurovascular regulation and cerebral amyloid angiopathy. *Bone*, 72, 709–727.

Milanese, C., Cerri, S., Ulusoy, A., Gornati, S. V., Plat, A., Gabriels, S., Blandini, F., Di Monte, D. A., Hoeijmakers, J. H., & Mastroberardino, P. G. (2018). Activation of the DNA damage response in vivo in synucleinopathy models of Parkinson's disease. *Cell Death & Disease*, 9, 818. https://doi.org/10.1038/s41419-018-0848-7

Moreau, C., Danel, V., Devedjian, J. C., Grolez, G., Timmerman, K., Laloux, C., Petrault, M., Moreau, C., Danel, V., Devedjian, J. C., Grolez, G., Timmerman, K., Laloux, C., Petrault, M., Gouel, F., Jonneaux, A., Dutheil, M., Lachaud, C., Lopes, R., … Devos, D. (2018). Could conservative iron chelation lead to neuroprotection in amyotrophic lateral sclerosis? *Antioxidants & Redox Signaling*, 29(8), 742–748. https://doi.org/10.1089/ars.2017.7493

Oexle, H., Gnaiger, E., & Weiss, G. (1999). Iron-dependent changes in cellular energy metabolism: Influence on citric acid cycle and oxidative phosphorylation. *Biochimica Et Biophysica Acta - Bioenergetics*, 1413, 99–107. https://doi.org/10.1016/S0005-2728(99)00088-2

Oh, S. W., Harris, J. A., Ng, L., Winslow, B., Cain, N., Mihalas, S., Wang, Q., Lau, C., Kuan, L., Henry, A. M., Mortrud, M. T., Ouellette, B., Nguyen, T. N., Sorensen, S. A., Slaughterbeck, C. R., Wakeman, W., Li, Y., Feng, D., Ho, A., … Zeng, H. (2014). A mesoscale connectome of the mouse brain. *Nature*, 508, 207–214. https://doi.org/10.1038/nature13186

Oliveira, M. A. P., Arreckx, S., Di Monte, D., Preciat, G. A., Ulusoy, A., & Fleming, R. M. T. (2019). The connectome is necessary but not sufficient for the spread of alpha -synuclein pathology in rats. *bioRxiv*. https://doi.org/10.1101/567222

Park, J. Y., Paik, S. R., Jou, I., & Park, S. M. (2008). Microglial phagocytosis is enhanced by monomeric α-synuclein, not aggregated α-synuclein: Implications for Parkinson's disease. *Glia*, 56, 1215–1223. https://doi.org/10.1002/glia.20691

Paumier, K. L., Luk, K. C., Manfredsson, F. P., Kanaan, N. M., Lipton, J. W., Collier, T. J., Steece-Collier, K., Kemp, C. J., Celano, S., Schulz, E., Sandoval, I. M., Fleming, S., Dirr, E., Polinski, N. K., Trojanowski, J. Q., Lee, V. M., & Sortwell, C. E. (2015). Intrastriatal injection of pre-formed mouse α-synuclein fibrils into rats triggers α-synuclein

pathology and bilateral nigrostriatal degeneration. *Neurobiology of Disease*, 82, 185–199. https://doi.org/10.1016/j.nbd.2015.06.003

Paxinos, G., & Franklin, K. B. J. (2003). *The Mouse Brain in Stereotaxic Coordinates*. Elsevier Academic Press.

Peelaerts, W., Bousset, L., Van der Perren, A., Moskalyuk, A., Pulizzi, R., Giugliano, M., Van den Haute, C., Melki, R., & Baekelandt, V. (2015). α-Synuclein strains cause distinct synucleinopathies after local and systemic administration. *Nature*, 522, 340–344. https://doi.org/10.1038/nature14547

Peng, Y., Wang, C., Xu, H., Liu, Y.-N., & Zhou, F. (2010). Binding of α-synuclein with Fe(III) and with Fe(II) and biological implications of the resultant complexes. *Journal of Inorganic Biochemistry*, 104, 365–370. https://doi.org/10.1016/j.jinorgbio.2009.11.005

Rossi, M., Ruottinen, H., Soimakallio, S., Elovaara, I., & Dastidar, P. (2013). Clinical MRI for iron detection in Parkinson's disease. *Clinical Imaging*, 37, 631–636. https://doi.org/10.1016/j.clinimag.2013.02.001

Saal, K. A., Koch, J. C., Tatenhorst, L., Szego, E. M., Ribas, V. T., Michel, U., Bähr, M., Tönges, L., & Lingor, P. (2015). AAV.shRNA-mediated downregulation of ROCK2 attenuates degeneration of dopaminergic neurons in toxin-induced models of Parkinson's disease in vitro and in vivo. *Neurobiology of Disease*, 73, 150–162. https://doi.org/10.1016/j.nbd.2014.09.013

Salami, A., Avelar-Pereira, B., Garzón, B., Sitnikov, R., & Kalpouzos, G. (2018). Functional coherence of striatal resting-state networks is modulated by striatal iron content. *NeuroImage*, 183, 495–503. https://doi.org/10.1016/j.neuroimage.2018.08.036

Schröder, N., Fredriksson, A., Vianna, M. R. M., Roesler, R., Izquierdo, I., & Archer, T. (2001). Memory deficits in adult rats following postnatal iron administration. *Behavioural Brain Research*, 124, 77–85. https://doi.org/10.1016/S0166-4328(01)00236-4

Shimozawa, A., Ono, M., Takahara, D., Tarutani, A., Imura, S., Masuda-Suzukake, M., Higuchi, M., Yanai, K., Hisanaga, S. I., & Hasegawa, M. (2017). Propagation of pathological α-synuclein in marmoset brain. *Acta Neuropathologica Communications*, 5, 12. https://doi.org/10.1186/s40478-017-0413-0

Smith, W. W. (2005). Synuclein phosphorylation enhances eosinophilic cytoplasmic inclusion formation in SH-SY5Y cells. *Journal of Neuroscience*, 25, 5544–5552. https://doi.org/10.1523/JNEUROSCI.0482-05.2005

Solé, V. A. A., Papillon, E., Cotte, M., Walter, P. H., & Susini, J. (2007). A multiplatform code for the analysis of energy-dispersive X-ray fluorescence spectra. *Spectrochimica Acta - Part B Atomic Spectroscopy*, 62, 63–68. https://doi.org/10.1016/j.sab.2006.12.002

Solntseva, E. I., Bukanova, J. V., Kondratenko, R. V., & Skrebitsky, V. G. (2015). Fe2+ and Fe3+ in micromolar concentrations modulate glycine-induced Cl− current in rat hippocampal neurons. *Brain Research Bulletin*, 115, 9–16. https://doi.org/10.1016/j.brainresbull.2015.04.004

Spillantini, M. G., Crowther, R. A., Jakes, R., Hasegawa, M., & Goedert, M. (1998). alpha-Synuclein in filamentous inclusions of Lewy bodies from Parkinson' s disease and dementia with Lewy bodies. *Proceedings of the National Academy of Sciences*, 95, 6469–6473. https://doi.org/10.1073/pnas.95.11.6469

Suzuki, W. A., Miller, E. K., & Desimone, R. (1997). Object and place memory in the macaque entorhinal cortex. *Journal of Neurophysiology*, 78, 1062–1081. https://doi.org/10.1152/jn.1997.78.2.1062

Tatenhorst, L., Eckermann, K., Dambeck, V., Fonseca-Ornelas, L., Walle, H., Lopes da Fonseca, T., Koch, J. C., Becker, S., Tönges, L., Bähr, M., Outeiro, T. F., Zweckstetter, M., & Lingor, P. (2016). Fasudil attenuates aggregation of α-synuclein in models of Parkinson's disease. *Acta Neuropathol Commun*, 4, 39. https://doi.org/10.1186/s40478-016-0310-y

Tatenhorst, L., Tönges, L., Saal, K.-A., Koch, J. C., Szegő, E. M., Bähr, M., & Lingor, P. (2014). Rho kinase inhibition by fasudil in the striatal 6-hydroxydopamine lesion mouse model of Parkinson disease. *Journal of Neuropathology and Experimental Neurology*, 73, 770–779. https://doi.org/10.1097/NEN.0000000000000095

Terada, M., Suzuki, G., Nonaka, T., Kametani, F., Tamaoka, A., & Hasegawa, M. (2018). The effect of truncation on prion-like properties of -synuclein. *Journal of Biological Chemistry*, 293, 13910–13920.

Tran, H. T., Chung, C.- H.-Y., Iba, M., Zhang, B., Trojanowski, J. Q., Luk, K. C., & Lee, V. M. Y. (2014). α-synuclein immunotherapy blocks uptake and templated propagation of misfolded α-synuclein and neurodegeneration. *Cell Reports*, 7, 2054–2065. https://doi.org/10.1016/j.celrep.2014.05.033

Uversky, V. N., Li, J., & Fink, A. L. (2001). Metal-triggered structural transformations, aggregation, and fibrillation of human α-synuclein: A possible molecular link between Parkinson's disease and heavy metal exposure. *Journal of Biological Chemistry*, 276, 44284–44296. https://doi.org/10.1074/jbc.M105343200

Valdinocci, D., Grant, G. D., Dickson, T. C., & Pountney, D. L. (2018). Epothilone D inhibits microglia-mediated spread of alpha-synuclein aggregates. *Molecular and Cellular Neuroscience*, 89, 80–94. https://doi.org/10.1016/j.mcn.2018.04.006

Vogel-Mikuš, K., Pongrac, P., & Pelicon, P. (2014). Micro-PIXE elemental mapping for ionome studies of crop plants. *International Journal of PIXE*, 24, 217–233. https://doi.org/10.1142/S0129083514400142

Volpicelli-Daley, L. A., Luk, K. C., Patel, T. P., Tanik, S. A., Riddle, D. M., Stieber, A., Meaney, D. F., Trojanowski, J. Q., & Lee, V.- M.-Y. (2011). Exogenous α-synuclein fibrils induce lewy body pathology leading to synaptic dysfunction and neuron death. *Neuron*, 72, 57–71. https://doi.org/10.1016/j.neuron.2011.08.033

Wang, S., Chu, C.-H., Stewart, T., Ginghina, C., Wang, Y., Nie, H., Guo, M., Wilson, B., Hong, J.-S., & Zhang, J. (2015). α-Synuclein, a chemoattractant, directs microglial migration via H2O2-dependent Lyn phosphorylation. *Proceedings of the National Academy of Sciences of the United States of America*, 112, E1926–E1935.

Winner, B., & Jappelli, R. (2011). In vivo demonstration that α-synuclein oligomers are toxic. *Proceedings of the National Academy of Sciences*, 108, 4194–4199.

Xia, Y., Zhang, G., Han, C., Ma, K., Guo, X., Wan, F., Kou, L., Yin, S., Liu, L., Huang, J., Xiong, N., & Wang, T. (2019). Microglia as modulators of exosomal alpha-synuclein transmission. *Cell Death and Disease*, 10, 174. https://doi.org/10.1038/s41419-019-1404-9

Zhang, B., Kehm, V., Gathagan, R., Leight, S. N., Trojanowski, J. Q., Lee, V.-M.-Y., & Luk, K. C. (2019). Stereotaxic targeting of alpha-synuclein pathology in mouse brain using preformed fibrils. *Methods in Molecular Biology*, 1948, 45–57. http://doi.org/10.1016/j.jns.2017.08.126

Zhang, W., Wang, T., Pei, Z., Miller, D. S., Wu, X., Block, M. L., Wilson, B., Zhang, W., Zhou, Y., Hong, J.-S., & Zhang, J. (2005). Aggregated α-synuclein activates microglia: A process leading to disease progression in Parkinson's disease. *The FASEB Journal*, 19(6), 533–542. http://doi.org/10.1096/fj.04-2751com

SUPPORTING INFORMATION

Additional supporting information may be found online in the Supporting Information section.

How to cite this article: Dauer née Joppe, K., Tatenhorst, L., Caldi Gomes, L., Zhang, S., Parvaz, M., Carboni, E., Roser, A.-E., El DeBakey, H., Bähr, M., Vogel-Mikuš, K., Wang Ip, C., Becker, S., Zweckstetter, M., & Lingor, P. (2021). Brain iron enrichment attenuates α-synuclein spreading after injection of preformed fibrils. *Journal of Neurochemistry*, 159, 554–573. https://doi.org/10.1111/jnc.15461